

Empirical metallicity-dependent calibrations of effective temperature against colours for dwarfs and giants based on interferometric data

Y. Huang^{1*}, X.-W. Liu^{1,2*}, H.-B. Yuan^{2†}, M.-S. Xiang¹, B.-Q. Chen^{1†}, H.-W. Zhang^{1,2}

¹Department of Astronomy, Peking University, Beijing 100871, People's Republic of China

²Kavli Institute for Astronomy and Astrophysics, Peking University, Beijing 100871, People's Republic of China

ABSTRACT

We present empirical metallicity-dependent calibrations of effective temperature against colours for dwarfs of luminosity classes IV and V and for giants of luminosity classes II and III, based on a collection from the literature of about two hundred nearby stars with direct effective temperature measurements of better than 2.5 per cent. The calibrations are valid for an effective temperature range 3,100 – 10,000 K for dwarfs of spectral types M5 to A0 and 3,100 – 5,700 K for giants of spectral types K5 to G5. A total of twenty-one colours for dwarfs and eighteen colours for giants of bands of four photometric systems, i.e. the Johnson ($UBVR_J I_J JHK$), the Cousins ($R_C I_C$), the Sloan Digital Sky Survey (SDSS, gr) and the Two Micron All Sky Survey (2MASS, JHK_s), have been calibrated. Restricted by the metallicity range of the current sample, the calibrations are mainly applicable for disk stars ($[\text{Fe}/\text{H}] \gtrsim -1.0$). The normalized percentage residuals of the calibrations are typically 2.0 and 1.5 per cent for dwarfs and giants, respectively. Some systematic discrepancies at various levels are found between the current scales and those available in the literature (e.g. those based on the infrared flux method IRFM or spectroscopy). Based on the current calibrations, we have re-determined the colours of the Sun. We have also investigated the systematic errors in effective temperatures yielded by the current on-going large scale low- to intermediate-resolution stellar spectroscopic surveys. We show that the calibration of colour ($g - K_s$) presented in the current work provides an invaluable tool for the estimation of stellar effective temperature for those on-going or upcoming surveys.

Key words: techniques: interferometric – techniques: photometric – stars: fundamental parameters – stars: abundances – stars: atmospheres

1 INTRODUCTION

The determination of effective temperatures of stars is of utmost importance in stellar astrophysics. Accurate stellar effective temperatures are essential for reliable estimates of stellar metallicity by spectroscopy. The distribution of stellar metallicities provide vital clues for the understanding of the Galactic chemical evolution. For high resolution spectroscopy, the effective temperature is required as an input parameter for the stellar abundance analysis and thus its uncertainties is propagated to the resultant elemental abundances. For low- and intermediate-resolution spectroscopy, the basic atmospheric parameters (i.e. effective temperature T_{eff} , surface gravity $\log g$ and metallicity $[\text{Fe}/\text{H}]$) are often determined simultaneously from the measured spectrum, say, for example, by spectral template matching (e.g. Lee et al. 2008; Luo et al. 2015; Xiang et al. 2015) and there may exist some degeneracies amongst the stellar

parameters thus deduced, in particular between T_{eff} and $[\text{Fe}/\text{H}]$. Therefore, accurate and model-independent estimation of T_{eff} is a critical step for stellar abundance determinations, either to minimize the uncertainties in the case of high resolution spectroscopy or to break the degeneracy in the case of low- and intermediate-resolution spectroscopy. As a basic stellar parameter, T_{eff} is also directly related to the observables of a star, such as its photometric colours, and the relations between T_{eff} and photometric colours are widely employed in a variety of astrophysical studies. For example, the relations are used to convert a stellar isochrone of a given (simple) stellar population, i.e. the locus of stellar luminosity L as a function of T_{eff} , yielded by theoretical stellar evolution models, to a relation in observable space, such as colour-magnitude diagrams (CMDs; Demarque & Larson 1964; Yi et al. 2001; Girardi et al. 2002, 2004; Dotter et al. 2008). Such CMDs have been widely applied to interpret photometric measurements of stellar clusters to determine their basic properties (e.g. age, distance and metallicity).

A variety of methods have been developed to estimate T_{eff} . For high resolution spectroscopy, techniques such as fitting the pro-

* E-mails: yanghuang@pku.edu.cn (YH); x.liu@pku.edu.cn (XWL)

† LAMOST Fellow

files of Balmer lines (Gray 1992; Heiter et al. 2002) or adjusting the “excitation balance” of Fe lines (Takeda et al. 2002; Santos et al. 2004) are often used. For low- and intermediate-resolution spectrophotometry, fitting the stellar continuum flux (over a wavelength range as wide as possible) with model atmosphere synthetic fluxes (e.g. Smalley 2005; Norris et al. 2013) or the strength of Balmer jump (Sokolov 1995) is generally used. All these indirect methods of T_{eff} estimation require however reliable stellar model atmospheres, and, as a consequence, lead to some model-dependent of the results.

The most popular and least model-dependent (or semi-direct) method for T_{eff} determination is the infrared flux method (IRFM), which is first developed by Blackwell & Shallis (1977). Since then, tremendous amount of work by many authors have used the IRFM to determine effective temperatures of stars (Alonso et al. 1996, 1999; Ramírez & Meléndez 2005; Casagrande et al. 2006; González Hernández & Bonifacio 2009; Casagrande et al. 2010). However, the lack of absolute zero-point calibration of the IRFM could induce some systematic errors, by as much as ~ 100 K, among the different studies (cf., e.g., the discussion of Casagrande et al. 2010).

Reliable estimates of T_{eff} can also be obtained from photometric colours using accurately calibrated metallicity-dependent T_{eff} -colour relations¹. The method allows one to accurately determine values of T_{eff} for large numbers of stars based on (relatively “cheap”) photometric measurements alone. This is extremely important in the current era of large scale surveys, with a number of large scale stellar spectroscopic surveys on-going, including the Sloan Extension for Galactic Understanding and Exploration (SEGUE; Yanny et al. 2009), the Radial Velocity Experiment (RAVE; Steinmetz et al. 2006), the Apache Point Observatory Galactic Evolution Experiment (APOGEE; Eisenstein et al. 2011), the LAMOST Spectroscopic Survey of the Galactic Anticenter (LSS-GAC; Liu et al. 2014, Yuan et al. 2014) and Gaia (Perryman et al. 2001). Those surveys are generating a huge amount of data that will dramatically improve our understanding of the formation and evolution of the Milky Way.

The key to a robust metallicity-dependent T_{eff} -colour relation is accurate, model-independent measurements of T_{eff} . For the moment, both theoretical model atmospheres (e.g. Bessell, Castelli & Plez 1998; Houdashelt, Bell & Sweigart 2000) and empirical measurements (e.g. Gratton, Carretta, & Castelli 1996; Weiss & Salaris 1999; Vandenberg & Clem 2003) are used to calibrate the relations. However, the synthetic broad-band colours derived from model atmospheres may deviate the real values due to some defects, for example, in the choice of microturbulence velocity, especially for cool stars (i.e. $T_{\text{eff}} \lesssim 4000$ K; Castelli 1999; Kučinskás et al. 2005; Casagrande & Vandenberg 2014) or in the treatment of convection of late-type giants (Kučinskás et al. 2005). As for the empirical approach, the source of error is mainly contributed by uncertainties in the estimates of T_{eff} , which may result, for example, as a consequence of adopting inappropriate stellar models in the case of indirect methods or the usage of an incorrect zero-point in the case of IRFM method. In order to construct a robust empirical metallicity-dependent T_{eff} -colour relation, accurate direct measurements of

T_{eff} are indispensable, preferably for a number of stars coverage wide ranges of stellar parameters, including the metallicity.

Direct measurements of stellar effective temperature are now available for a large number of stars for which their angular diameters directly measured using long-baseline optical/infrared interferometry (LBOI; e.g. Code et al. 1976). With angular diameters measurement from LBOI, linear radii can be derived when the geometric parallaxes (e.g. from the Hipparcos; van Leeuwen 2007) are also available. Then, the linear radii combined with bolometric flux measurements yield directly the stellar effective temperatures through the Stefan-Boltzmann equation (Mozurkewich et al. 2003, hereafter M03; Baines et al. 2009; Boyajian et al. 2009, 2012a,b, 2013, hereafter B12a, B12b and B13, respectively; Creevey et al. 2012; White et al. 2013). Due to the progress in observations in the past few years, stellar angular diameters can now be measured to an accuracy of better than 5.0 per cent, implying T_{eff} measurements of better than 2.5 per cent. Those data have however not been fully utilized to calibrate the aforementioned, very important, empirical metallicity-dependent T_{eff} -colours relations. Quite recently, B12b derive the metallicity-dependent T_{eff} -colour relations in the Johnson *BVJHK* bands based on a small sample of 40 G/K/M dwarfs with direct angular diameter measurement of better than 5 per cent, while B13 do so based on a sample of over one hundred A to M dwarfs with direct T_{eff} measurements. In the latter study, the effects of metallicity are considered for colour ($B - V$) only. Both calibrations are restricted to population I (i.e. $[\text{Fe}/\text{H}] > -1.0$) dwarfs of luminosity classes IV and V.

In this paper, we improve, on the basis of work by B12a,b and B13, the metallicity-dependent empirical T_{eff} -colour relations for dwarfs by adding more metal-poor stars with direct T_{eff} measurements to the calibration sample. Accurate estimates of the interstellar extinction are also made for all calibration stars. In addition, we present similar calibration for giants based on available direct T_{eff} measurements for those types of star. The paper is organized as follows. In Section 2 we introduce the calibration sample compiled from the literature and the extinction determinations for the sample stars. The empirical calibrations of T_{eff} versus colours and $[\text{Fe}/\text{H}]$ are presented in Section 3. Comparisons with previous work and applications of the newly derived relations are given in Sections 4 to 6, respectively. Finally, we conclude in Section 7.

2 DATA

In B13, direct measurements of T_{eff} for 125 dwarf stars (luminosity classes: IV/V) are collected from their surveys of stellar diameters and effective temperatures (B12a, B12b and B13) as well as from 24 other publications. We take 121 stars from the B13 sample, discarding two stars with T_{eff} errors greater than 2.5 per cent and another two with incommensurate measurements of T_{eff} amongst the different work. On top of this, we collect another 13 dwarf stars with direct T_{eff} measurements from 6 publications. Thus the sample of dwarfs employed in the current work consists of a total of 134 stars with direct T_{eff} measurements of better than 2.5 per cent. The sample stars span spectral types from M5 to A0, with T_{eff} ranging from $\sim 3, 100$ to 10,000 K. For giant stars (luminosity classes: II/III), direct T_{eff} measurements, also accurate to better than 2.5 per cent, of 61 stars are compiled from 9 publications. The giants span spectral types from M5 to G5, with T_{eff} ranging from $\sim 3, 100$ to 5,700 K.

¹ With accurate enough photometric data, one can determine T_{eff} without the knowledge of (spectroscopic) metallicity if suitable colour measurements are available (e.g. $U - B$ for early, hot OB stars, $V - K$ for late, cool KM stars). In those cases, T_{eff} can be determined by iteration, assuming, for example, an initial value of metallicity such as that of the Sun.

Table 1: Compiled data of dwarf and giant sample stars employed in the current work

Name	Spectral type	U (mag)	B (mag)	V (mag)	R_J (mag)	I_J (mag)	R_C (mag)	I_C (mag)	J (mag)	H (mag)	K (mag)	$E(B - V)$ (mag)	T_{eff} (K)	$\sigma_{T_{\text{eff}}}$ (K)	[Fe/H]	Flag1	Flag2	Flag3
Dwarf stars																		
HD173740	M5V	–	11.28	9.69	–	–	–	–	5.72	5.24	4.98	0.001	3104	28	–0.54	B12b	PASTEL	2
HIP087937	M4Ve	–	11.26	9.53	–	–	8.32	6.76	5.30	4.77	4.50	0.002	3222	10	–0.15	B12b	PASTEL	4
HD173739	M3V	–	10.44	8.90	–	–	–	–	5.19	4.68	4.46	0.001	3407	15	–0.49	B12b	B12	4
HIP086162	M3V	–	10.65	9.15	–	–	–	–	5.37	4.75	4.54	0.000	3413	28	0.00	B12b	PASTEL	1
HIP057087	M3V	–	12.17	10.65	–	–	–	–	6.90	6.32	6.07	0.000	3416	53	0.04	B12b	B12	3
HIP074995	M2.5V	–	12.19	10.58	8.89	7.46	9.45	8.06	6.68	6.09	5.83	0.000	3442	54	–0.10	B12b	B12	3
HD095735	M2V	–	8.91	7.42	5.94	4.77	6.40	5.28	4.11	3.55	3.34	0.023	3464	15	–0.31	B12b	PASTEL	1
HIP054211	M2V	–	10.27	8.73	7.26	6.20	–	–	5.55	4.94	4.76	0.012	3497	39	–0.43	B12b	PASTEL	1
HD001326	M1.5V	–	9.63	8.07	6.69	5.53	–	–	4.86	4.25	4.02	0.000	3567	11	–0.36	B12b	B12	0
HD119850	M1.5V	–	9.93	8.50	7.06	5.92	7.49	6.39	5.26	4.64	4.46	0.000	3618	31	–0.10	B12b	PASTEL	1
HD217987	M0.5V	–	8.82	7.34	–	–	6.35	5.31	4.20	3.60	3.36	0.004	3676	35	–0.22	B12b	PASTEL	1
HD199305	M0.5V	–	10.03	8.57	7.19	6.13	–	–	5.52	4.81	4.64	0.004	3692	22	–0.13	B12b	PASTEL	1
HD216899	M1.5V	–	10.19	8.68	–	–	7.69	6.57	5.41	4.78	4.58	0.000	3713	11	0.06	B12b	B12	0
HD036395	M1.5V	–	9.44	7.97	6.53	5.39	6.98	5.89	4.77	4.06	3.86	0.000	3801	9	0.21	B12b	PASTEL	1
HD079211	K7V	–	9.04	7.70	–	–	–	–	4.78	4.30	4.15	0.001	3867	37	–0.40	B12b	MILES	2
HD079210	M0V	–	9.05	7.64	–	–	–	–	4.89	4.25	4.09	0.000	3907	35	–0.18	B12b	B12	3
HD201092	K7V	8.60	7.38	6.02	4.87	4.07	–	–	3.58	2.93	2.73	0.000	3932	25	–0.39	B12b	PASTEL	1
HD088230	K7V	–	7.92	6.57	5.35	4.55	–	–	3.98	3.32	3.19	0.005	4085	14	–0.03	B12b	PASTEL	1
HD201091	K5V	7.51	6.39	5.23	4.20	3.56	–	–	3.16	2.61	2.40	0.000	4361	17	–0.25	B12b	PASTEL	2
HD131977	K4V	7.95	6.88	5.78	4.85	4.28	4.96	4.32	3.82	3.27	3.15	0.000	4507	58	0.07	B12b	PASTEL	1
HD209100	K5V	–	5.75	4.69	3.81	3.25	4.05	3.53	2.83	2.30	2.18	0.000	4555	24	–0.08	B12b	PASTEL	1
HD122563	F8IV	7.26	6.92	6.06	5.27	4.72	5.55	5.04	4.29	3.74	3.67	0.044	4598	42	–2.65	R13	PASTEL	1
HD016160	K3V	–	6.79	5.82	4.99	4.46	5.24	4.75	4.07	3.52	3.45	0.000	4662	17	–0.11	B12b	PASTEL	1
HD219134	K3V	7.34	6.47	5.50	4.69	4.18	–	–	3.84	3.39	3.22	0.023	4699	16	0.08	B12b	PASTEL	1
HD222404	K1V	5.19	4.24	3.21	2.46	–	–	–	–	–	–	0.000	4744	21	0.12	Ba09	PASTEL	1
HD103095	K1V	7.36	7.18	6.44	5.78	5.33	–	–	4.95	4.44	4.40	0.004	4791	28	–1.33	B13	PASTEL	1
HD198149	K0IV	4.91	4.31	3.40	2.74	2.25	–	–	1.89	1.49	1.28	0.011	4835	37	–0.12	B13	PASTEL	1
HD188512	G8IV-V	5.06	4.58	3.72	3.06	2.57	3.26	2.83	2.26	1.71	1.71	0.000	4920	102	–0.18	B13	PASTEL	1
HD004628	K2V	–	6.62	5.75	4.98	4.51	5.21	4.76	4.24	3.72	3.61	0.004	4950	14	–0.27	B12b	PASTEL	1
HD023249	K1IV	–	4.46	3.54	2.82	2.32	3.02	2.59	1.96	1.52	1.40	0.000	4955	30	0.15	B13	PASTEL	1
HD011964	G9V	–	7.23	6.41	–	–	5.97	5.56	5.02	4.64	4.49	0.002	5013	62	0.12	B13	PASTEL	1
HD003651	K0V	–	6.71	5.86	5.21	4.82	–	–	4.48	4.03	3.97	0.000	5046	86	0.15	B13	PASTEL	1
HD022049	K2V	–	4.62	3.74	3.01	2.55	3.23	2.79	2.20	1.75	1.65	0.000	5077	35	–0.06	B12b	PASTEL	1
HD026965	K1Ve	–	5.25	4.43	3.74	3.29	3.96	3.54	2.95	2.48	2.41	0.000	5147	14	–0.28	B12b	PASTEL	1
HD075732	K0IV-V	–	6.80	5.94	–	–	–	–	4.59	4.14	4.07	0.000	5172	18	0.37	B13	PASTEL	1
HD158633	K0V	–	7.10	6.36	–	–	–	–	–	–	–	0.023	5203	46	–0.47	B13	PASTEL	1
HD128621	K2IV	2.84	2.19	1.30	–	–	–	–	–0.01	–0.41	–0.61	0.015	5232	8	0.24	B13	PASTEL	1
HD182736	G0IV	–	7.63	6.86	–	–	–	–	5.53 ^a	–	5.04 ^a	0.047	5239	37	–0.11	B13	PASTEL	1
HD010476	K0V	–	6.08	5.24	4.55	4.12	–	–	3.85	3.44	3.21	0.000	5242	12	–0.04	B13	PASTEL	1
HD185144	K0V	5.86	5.49	4.69	4.04	3.63	–	–	3.32	3.04	2.78	0.000	5246	26	–0.23	B12b	PASTEL	1
HD021019	G2V	–	6.81	6.13	–	–	–	–	–	–	–	0.023	5261	65	–0.44	B13	PASTEL	1
HD010700	G8V	–	4.22	3.50	2.88	2.41	3.06	2.68	2.16	1.72	1.68	0.000	5290	39	–0.52	B13	PASTEL	1
HD173701	K0V	–	8.26	7.45	–	–	–	–	6.11 ^a	5.73 ^a	5.69 ^a	0.029	5297	53	0.33	B13	PASTEL	1
HD101501	G8V	6.31	6.08	5.34	4.73	4.37	–	–	4.02	3.61	3.60	0.000	5309	27	–0.03	B13	PASTEL	1
HD000166	G8V	–	6.89	6.14	–	–	–	–	–	–	–	0.000	5327	39	0.11	B13	PASTEL	1
HD149661	K0V	7.00	6.55	5.74	5.13	4.74	5.30	4.89	4.32	3.86	3.83	0.000	5337	41	0.05	B12b	PASTEL	1
HD006582	G5V	–	5.79	5.12	4.51	4.11	–	–	3.84	3.38	3.35	0.019	5348	26	–0.88	B12b	PASTEL	1
HD082885	G8V	–	6.18	5.41	4.79	4.42	–	–	4.14	3.77	3.70	0.000	5376	43	0.36	B13	PASTEL	1
HD217107	G8IV-V	–	6.89	6.15	–	–	–	–	–	–	–	0.003	5391	40	0.36	B13	PASTEL	1
HD010780	K0V	–	6.44	5.63	4.99	4.60	–	–	4.31	3.88	3.84	0.000	5398	75	0.02	B12b	PASTEL	1
HD117176	G5V	5.90	5.65	4.95	4.35	3.96	–	–	3.64	3.25	3.24	0.010	5406	64	–0.06	B13	PASTEL	1
HD165341	K0Ve	–	4.95	4.12	–	–	3.45	3.01	–	–	2.29	0.026	5407	52	0.04	B12b	PASTEL	1
HD195564	G2V	–	6.32	5.64	–	–	5.27	4.91	–	–	–	0.003	5421	118	0.05	B13	PASTEL	1
HD010697	G3Va	–	6.95	6.23	–	–	–	–	4.97	4.66	4.58	0.009	5442	65	0.15	B13	PASTEL	1
HD190360	G7IV-V	–	6.41	5.70	–	–	–	–	4.45	4.11	4.05	0.002	5461	75	0.23	B13	PASTEL	1

Table 1: Continued.

Name	Spectral type	U (mag)	B (mag)	V (mag)	R_J (mag)	I_J (mag)	R_C (mag)	I_C (mag)	J (mag)	H (mag)	K (mag)	$E(B - V)$ (mag)	T_{eff} (K)	$\sigma_{T_{\text{eff}}}$ (K)	[Fe/H]	Flag1	Flag2	Flag3
HD131156	G7V	5.60	5.31	4.54	3.91	3.48	–	–	3.01	2.59	2.57	0.001	5483	32	−0.15	B13	PASTEL	1
HD161797	G5IV	4.56	4.17	3.42	2.89	2.51	–	–	2.18	1.81	1.77	0.000	5502	55	0.25	B13	PASTEL	1
HD086728	G4V	–	6.01	5.35	–	–	–	–	–	–	–	0.000	5619	44	0.21	B13	PASTEL	1
HD182572	G8IV	6.25	5.86	5.10	–	–	–	–	3.82	3.54	3.48	0.020	5643	84	0.39	B13	PASTEL	1
HD038858	G2V	–	6.56	5.93	–	–	–	–	–	–	–	0.012	5646	45	−0.23	B13	PASTEL	1
HD150680	G2IV	3.50	3.31	2.70	2.22	1.93	–	–	1.67	1.32	1.29	0.036	5656	63	0.01	B13	PASTEL	1
HD136202	F8IV	–	5.57	5.04	4.63	4.37	4.73	4.43	–	–	–	0.008	5661	87	−0.05	B13	PASTEL	1
HD186427	G3V	7.06	6.85	6.19	5.75	5.42	–	–	5.04	4.70	4.65	0.002	5678	66	0.07	B13	PASTEL	1
HD140538	G5V	–	6.55	5.87	–	–	5.46	5.11	–	–	–	0.005	5692	74	0.05	B13	PASTEL	1
HD109358	G0V	4.90	4.85	4.26	3.72	3.42	–	–	3.23	2.85	2.84	0.002	5700	95	−0.21	B13	PASTEL	1
HD217014	G3V	6.39	6.17	5.50	4.96	4.62	–	–	4.36	4.03	3.99	0.000	5706	95	0.21	B13	PASTEL	1
HD140283 ^b	F3VI	7.52	7.71	7.22	6.63	6.32	6.87	6.51	6.04	5.69	5.66	0.000	5720	29	−2.46	R13	PASTEL	1
HD020630	G5V	–	5.51	4.83	4.26	3.91	4.44	4.10	3.71	3.35	3.34	0.003	5723	76	0.04	B13	PASTEL	1
HD157214	G0V	6.07	6.00	5.38	4.87	4.53	–	–	4.22	3.86	3.84	0.000	5738	48	−0.39	B13	MILES	2
HD186408	G1.5V	6.79	6.59	5.95	5.50	5.17	–	–	4.91	4.44	4.52	0.000	5760	57	0.07	B13	PASTEL	1
HD190406	G0V	–	6.41	5.80	–	–	–	–	–	–	–	0.000	5763	49	0.05	B13	PASTEL	1
HD034411	G1V	–	5.30	4.69	4.16	3.85	–	–	3.61	3.33	3.28	0.007	5774	44	0.04	B13	PASTEL	1
HD022879 ^b	F9V	7.02	7.11	6.60	6.14	5.82	6.28	5.97	5.57	5.25	5.22	0.026	5786	16	−0.84	R13	PASTEL	1
HD130948	F9IV-V	–	6.41	5.85	–	–	–	–	4.79	4.53	4.48	0.000	5787	57	−0.05	B13	PASTEL	1
HD128620	G2V	0.72	0.50	−0.15	–	–	−0.47	−0.77	−1.14	−1.32	−1.42	0.047	5793	7	0.20	B13	PASTEL	1
HD019373	G0IV-V	–	4.65	4.05	3.52	3.23	–	–	3.06	2.73	2.69	0.000	5832	33	0.08	B13	PASTEL	1
HD206860	G0IV-V	–	6.53	5.94	–	–	–	–	–	–	–	0.000	5860	83	−0.08	B13	PASTEL	1
HD002151	G2IV	3.47	3.37	2.76	2.26	1.92	2.42	2.10	1.71	1.39	1.34	0.011	5872	44	−0.11	N07	PASTEL	1
HD039587	G0IV-V	–	5.00	4.41	3.90	3.59	–	–	3.34	3.04	2.97	0.000	5898	25	−0.04	B13	PASTEL	1
HD177153	G0V	–	7.76	7.20	–	–	–	–	6.20 ^a	5.92 ^a	5.86 ^a	0.001	5909	69	−0.07	B13	PASTEL	1
HD019994	F8.5V	–	5.55	5.00	–	–	4.66	4.37	–	–	–	0.020	5916	98	0.20	B13	PASTEL	1
HD162003	F5IV-V	–	5.01	4.58	4.20	3.97	–	–	3.70	3.47	3.43	0.000	5928	81	−0.07	B13	PASTEL	1
HD114710	G0V	4.92	4.84	4.26	3.77	3.47	–	–	3.22	2.95	2.89	0.000	5957	29	0.03	B13	PASTEL	1
HD005015	F8V	–	5.35	4.82	4.34	4.04	–	–	3.85	3.56	3.54	0.001	5965	35	0.01	B13	PASTEL	1
HD004614	F9V	–	3.95	3.38	2.90	2.55	–	–	2.33	2.01	1.95	0.018	5973	8	−0.30	B13	PASTEL	1
HD022484	F9IV-V	–	4.79	4.24	3.76	3.45	3.94	3.63	3.28	3.00	2.91	0.014	5998	39	−0.10	B13	PASTEL	1
HD121370	G0IV	3.46	3.26	2.68	2.24	1.95	–	–	1.70	1.38	1.37	0.000	6012	45	0.24	B13	PASTEL	1
HD102870	F8.5IV-V	4.26	4.15	3.60	3.12	2.84	3.28	2.99	2.63	2.35	2.33	0.000	6054	13	0.13	B13	PASTEL	1
HD175726	G5V	–	7.18	6.63	–	–	–	–	5.73 ^a	5.40 ^a	5.37 ^a	0.027	6067	67	−0.04	B13	PASTEL	1
HD006210	F6V	–	6.22	5.72	–	–	–	–	–	–	–	0.038	6089	35	−0.17	B13	PASTEL	1
HD215648	F6V	4.62	4.65	4.16	3.74	3.44	–	–	3.21	3.06	2.92	0.009	6090	22	−0.29	B13	PASTEL	1
HD009826	F8V	–	4.64	4.10	3.64	3.35	–	–	3.17	2.99	2.85	0.000	6104	75	0.09	B13	PASTEL	1
HD069897	F6V	–	5.53	5.08	–	–	–	–	4.15	3.93	3.90	0.020	6130	58	−0.28	B13	PASTEL	1
HD016895	F7V	–	4.54	4.07	3.63	3.34	–	–	3.32	3.06	2.97	0.019	6153	25	0.00	B13	PASTEL	1
HD187637	F5V	–	8.03	7.52	–	–	–	–	6.60 ^a	6.34 ^a	6.32 ^a	0.002	6155	85	−0.14	B13	PASTEL	1
HD222368	F7V	4.61	4.62	4.11	3.68	3.37	3.82	3.54	–	–	–	0.005	6192	26	−0.14	B13	PASTEL	1
HD090839	F8V	–	5.29	4.79	4.32	4.06	–	–	3.83	3.57	3.53	0.016	6203	56	−0.13	B13	PASTEL	1
HD126660	F7V	4.53	4.52	4.03	3.62	3.38	–	–	3.09	2.86	2.82	0.009	6211	19	−0.04	B13	PASTEL	1
HD168151	F5V	–	5.39	5.02	–	–	–	–	4.09	3.87	3.84	0.023	6221	39	−0.32	B13	PASTEL	1
HD142860	F6V	4.31	4.34	3.86	3.37	3.13	–	–	2.93	2.64	2.65	0.000	6222	13	−0.20	B13	PASTEL	1
HD082328	F5.5IV-V	–	3.57	3.13	2.70	2.44	–	–	2.27	2.02	2.01	0.017	6238	10	−0.18	B13	PASTEL	1
HD084937 ^b	F5VI	8.47	8.67	8.31	7.96	7.69	–	–	7.38	7.13	7.09	0.004	6275	17	−2.12	R13	PASTEL	2
HD181420	F2V	–	6.97	6.54	–	–	–	–	5.79 ^a	5.55 ^a	5.55 ^a	0.010	6283	106	0.00	B13	PASTEL	1
HD219623	F8V	–	6.10	5.58	–	–	–	–	–	–	–	0.000	6285	94	0.02	B13	PASTEL	1
HD173667	F5.5IV-V	4.58	4.58	4.14	3.76	3.52	–	–	3.29	3.07	3.03	0.016	6296	19	−0.05	B13	PASTEL	1
HD210027	F5V	4.17	4.20	3.76	3.36	3.11	–	–	2.98	2.71	2.66	0.000	6324	139	−0.18	B13	PASTEL	1
HD016765	F7V	–	6.23	5.71	–	–	–	–	–	–	–	0.000	6356	46	−0.15	B13	B13	3
HD128167	F4V	4.76	4.84	4.47	4.13	3.94	–	–	3.65	3.50	3.49	0.000	6435	50	−0.40	B13	PASTEL	1
HD030652	F6IV-V	–	3.60	3.15	2.74	2.49	2.89	2.64	2.34	2.14	2.07	0.013	6441	19	0.01	B13	PASTEL	1
HD089449	F6VI/V	5.26	5.25	4.80	4.35	4.12	–	–	3.84	–	3.65	0.000	6450	140	0.09	M13	PASTEL	1
HD164259	F2V	–	4.98	4.60	4.27	4.09	4.38	4.16	3.86	3.70	3.67	0.007	6454	113	−0.12	B13	PASTEL	1

Table 1: Continued.

Name	Spectral type	U (mag)	B (mag)	V (mag)	R_J (mag)	I_J (mag)	R_C (mag)	I_C (mag)	J (mag)	H (mag)	K (mag)	$E(B - V)$ (mag)	T_{eff} (K)	$\sigma_{T_{\text{eff}}}$ (K)	[Fe/H]	Flag1	Flag2	Flag3
HD048737	F5IV-V	-	3.78	3.35	2.96	2.74	-	-	2.57	1.87	2.30	0.003	6478	21	0.14	B13	B13	4
HD061421	F5IV-V	-	0.73	0.33	-0.08	-0.30	0.09	-0.14	-0.41	-0.51	-0.60	0.014	6582	16	-0.01	B13	PASTEL	1
HD120136	F7IV-V	5.02	4.98	4.50	4.09	3.85	-	-	3.61	3.40	3.35	0.000	6620	67	0.29	B13	PASTEL	1
HD049933	F2V	-	6.14	5.75	-	-	-	-	4.90	4.71	4.67	0.006	6635	90	-0.39	B13	PASTEL	1
HD081937	F0IV	-	4.00	3.67	3.33	3.15	-	-	3.01	3.00	2.82	0.000	6651	27	0.17	B13	B13	3
HD058946	F0V	-	4.50	4.18	3.86	3.67	-	-	3.58	3.34	3.36	0.000	6738	55	-0.25	B13	B13	0
HD218396	F0V	-	6.22	5.96	-	-	-	-	5.46	5.30	5.28	0.006	7163	84	-9.00	B13	-	4
HD187642	A7V	0.96	0.89	0.69	0.57	0.46	0.58	0.46	0.33	0.23	0.23	0.023	7361	91	-0.24	M03	PASTEL	1
HD219080	F1V	4.55	4.56	4.33	4.09	3.98	-	-	3.90	-	3.75	0.062	7380	90	-0.02	M13	PASTEL	1
HD128898	A7VpSrCrE	3.49	3.38	3.15	2.93	2.84	3.03	2.78	2.83	2.72	2.74	0.012	7420	170	0.13	Ba08	N94	4
HD222603	A7V	4.79	4.72	4.51	4.33	4.23	4.39	4.17	4.10	4.20	4.00	0.000	7734	80	-9.00	B13	-	3
HD210418	A2V	3.67	3.58	3.52	3.47	3.44	3.46	3.42	3.37	3.37	3.33	0.011	7872	82	-0.38	B13	PASTEL	1
HD097603	A5IV	-	2.68	2.56	2.43	2.40	-	-	2.33	2.27	2.27	0.000	7889	60	-0.18	B13	B13	3
HD141795	A2mV	-	3.81	3.66	3.59	3.55	3.61	3.56	-	-	-	0.012	7928	88	0.32	B13	PASTEL	1
HD118098	A2Van	3.58	3.50	3.38	3.31	3.25	3.32	3.26	3.18	3.05	3.06	0.000	8097	43	-0.05	B13	PASTEL	1
HD005448	A6V	4.12	3.97	3.86	3.71	3.63	-	-	3.57	3.50	3.49	0.004	8320	150	0.03	M13	M12	2
HD216956	A4V	1.19	1.15	1.08	1.04	1.04	1.04	1.03	1.00	1.04	0.96	0.024	8459	44	0.34	B13	PASTEL	1
HD213558	A1V	3.69	3.70	3.71	3.73	3.77	-	-	-	-	-	0.019	9050	157	-9.00	B13	-	4
HD177724	A0IV-V	2.92	2.94	2.95	2.95	2.96	-	-	2.92	3.02	2.91	0.014	9078	86	-0.52	B13	B13	4
HD095418	A1IV	-	2.24	2.29	2.25	2.31	-	-	2.33	2.34	2.34	0.026	9193	56	0.16	B13	PASTEL	1
HD097633	A2V	3.40	3.33	3.35	3.32	3.34	-	-	3.34	-	3.30	0.000	9480	120	-0.03	M13	PASTEL	1
HD172167	A0V	0.03	0.03	0.03	0.07	0.10	0.04	0.03	0.00	0.00	0.00	0.000	9657	119	-0.62	M03	PASTEL	1
HD048915	A0Va	-	-1.46	-1.46	-1.46	-1.43	-1.41	-1.40	-1.34	-1.33	-1.31	0.000	9711	23	0.34	B13	PASTEL	1
Giant stars																		
HD175865	M5III	7.00	5.59	4.00	1.95	0.04	-	-	-0.90	-1.80	-2.08	0.000	3174	41	0.14	M03	MILES	2
HD132813	M4.5III	7.86	6.19	4.54	2.69	0.97	-	-	0.19	-0.78	-1.00	0.000	3281	45	-9.00	M03	-	3
HD042995	M3III	6.42	4.78	3.20	1.73	0.44	-	-	-0.35	-1.23	-1.44	0.027	3462	43	0.04	M03	PASTEL	4
HD011695	M4III	7.59	5.89	4.33	2.62	1.13	2.94	0.46	0.50	-0.44	-0.65	0.026	3550	50	-9.00	W04	-	2
HD018884	M1.5IIIa	5.55	3.70	2.17	0.91	-0.15	1.30	0.35	-0.72	-1.47	-1.71	0.115	3578	53	-0.22	M03	PASTEL	3
HD112300	M3III	6.61	4.84	3.28	1.79	0.48	2.31	1.08	-0.24	-1.07	-1.25	0.031	3602	44	-0.16	M03	PASTEL	3
HD102212	M1IIIab	7.32	5.54	4.04	2.79	1.78	3.10	1.31	1.09	0.25	0.07	0.000	3610	53	-0.41	M03	K12	3
HD216386	M2.5IIIaF	7.20	5.44	3.79	2.37	1.18	2.60	0.53	0.44	-0.38	-0.64	0.000	3639	47	-9.00	M03	-	3
HD100029	M0III	7.44	5.47	3.85	2.54	1.55	-	-	0.87	0.18	-0.12	0.000	3675	46	-9.00	M03	-	3
HD025025	M1IIIbCA-	6.52	4.54	2.94	1.68	0.68	2.06	0.28	0.07	-0.74	-0.93	0.000	3703	54	-9.00	M03	-	3
HD146051	M0.5III	6.30	4.34	2.75	1.46	0.43	1.83	0.91	-0.24	-0.98	-1.26	0.000	3721	47	0.32	M03	PASTEL	2
HD183439	M0III	7.77	5.95	4.45	3.24	2.27	-	-	1.53	-	0.52	0.000	3769	46	-0.38	M03	PASTEL	1
HD089758	M0III	6.48	4.59	3.02	1.73	0.78	-	-	0.09	-0.69	-0.86	0.011	3793	47	0.00	M03	PASTEL	3
HD017709	K5III	7.83	5.93	4.40	3.23	2.31	-	-	1.73	-	0.71	0.040	3799	47	-0.36	M03	PASTEL	4
HD080493	K7IIIab	6.13	4.26	2.82	1.67	0.85	-	-	0.23	-0.53	-0.68	0.105	3836	47	-0.26	M03	PASTEL	1
HD131873	K4III	5.32	3.55	2.08	0.97	0.21	-	-	-0.45	-	-1.39	0.000	3849	47	-0.29	M03	PASTEL	1
HD189319	M0III	6.88	4.96	3.41	2.23	1.32	-	-	0.68	-	-0.26	0.019	3836	36	-0.31	M03&W06	PASTEL	4
HD029139	K5III	4.20	2.30	0.78	-0.43	-1.35	-	-	-1.89	-2.62	-2.86	0.025	3871	48	-0.22	M03	PASTEL	1
HD069267	K4III	6.32	4.62	3.23	2.19	1.47	2.51	1.87	0.98	0.23	0.10	0.098	4012	52	-0.16	M03	PASTEL	1
HD164058	K5III	5.26	3.43	1.99	0.90	0.12	-	-	-0.51	-	-1.38	0.076	4013	52	-0.11	M03	PASTEL	1
HD098262	K3III	6.44	4.89	3.49	2.43	1.73	-	-	1.18	-	0.31	0.000	4091	50	-0.11	M03	PASTEL	1
HD124897	K1.5IIIFe	2.46	1.18	-0.05	-1.03	-1.68	-0.76	-1.34	-2.22	-2.91	-3.00	0.000	4226	53	-0.55	M03	PASTEL	1
HD023319	K2.5III	7.03	5.73	4.55	-	-	3.95	3.44	-	-	-	0.012	4294	58	0.30	C12	PASTEL	1
HD073108	K1III	6.94	5.78	4.61	3.72	3.09	-	-	2.48	1.94	1.88	0.000	4336	99	-0.23	Ba10b	PASTEL	1
HD102328	K3III	8.05	6.56	5.28	-	-	-	-	-	-	-	0.000	4358	97	0.09	Ba10b	PASTEL	1
HD003627	K3III	5.90	4.44	3.19	2.29	1.66	-	-	1.15	-	0.42	0.030	4392	54	0.26	M03	PASTEL	1
HD085503	K3III	6.42	5.03	3.83	2.93	2.37	-	-	1.92	-	1.21	0.017	4433	51	0.34	R13	PASTEL	1
HD160290	K1III	7.57	6.51	5.36	-	-	-	-	-	-	-	0.000	4493	98	-0.21	Ba10b	PASTEL	1
HD012929	K2III	4.15	3.05	1.92	1.08	0.50	-	-	0.04	-0.54	-0.64	0.029	4493	55	-0.23	M03	PASTEL	1
HD137759	K2III	5.56	4.35	3.21	2.45	1.87	-	-	1.36	-	0.67	0.025	4545	110	0.09	Ba11	PASTEL	1
HD096833	K1III	5.07	3.98	2.88	2.08	1.55	-	-	1.12	-	0.42	0.042	4563	42	-0.07	M03&Ba10a	PASTEL	1
HD140573	K2IIIbCN1	5.08	3.82	2.65	1.82	1.25	2.05	1.55	0.74	0.18	0.06	0.000	4558	56	0.05	M03	PASTEL	1

 T_{eff} -colour-metallicity relations

Table 1: Continued.

Name	Spectral type	U (mag)	B (mag)	V (mag)	R_J (mag)	I_J (mag)	R_C (mag)	I_C (mag)	J (mag)	H (mag)	K (mag)	$E(B - V)$ (mag)	T_{eff} (K)	$\sigma_{T_{\text{eff}}}$ (K)	[Fe/H]	Flag1	Flag2	Flag3
HD003712	K0IIIa	4.13	3.07	1.98	1.26	0.73	–	–	0.35	–	–0.28	0.082	4602	57	–0.15	M03	PASTEL	1
HD095689	K0IIIa	3.77	2.85	1.78	0.98	0.40	–	–	–0.01	–0.61	–0.64	0.002	4637	62	–0.20	M03	PASTEL	1
HD175955	K0III	–	7.95	6.84	–	–	–	–	5.00 ^a	–	4.32 ^a	0.057	4688	66	0.12	H12	PASTEL	1
HD215665	G8IIIa*	5.69	4.79	3.77	3.04	2.58	–	–	2.21	–	1.63	0.050	4699	71	–0.08	M03	PASTEL	1
HD188310	G9III	6.64	5.75	4.70	–	–	4.17	3.69	–	–	–	0.000	4742	26	–0.32	Ba09	PASTEL	1
HD197989	K0III	4.30	3.44	2.42	1.70	1.17	–	–	0.72	0.19	0.09	0.012	4756	59	–0.13	M03	PASTEL	1
HD177151	K0III	–	7.97	6.99	–	–	–	–	5.30 ^a	4.81 ^a	4.71 ^a	0.016	4761	70	–0.09	H12	PASTEL	1
HD028307	K0IIIb	5.52	4.79	3.84	–	–	–	–	2.29	–	1.73	0.000	4811	50	0.11	B09	PASTEL	1
HD186815	K2III	–	7.13	6.26	–	–	–	–	–	–	–	0.006	4823	81	–0.32	Ba10b	B10	2
HD221345	G8III	6.93	6.09	5.10	–	–	–	–	–	–	–	0.039	4826	40	–0.37	Ba09	PASTEL	1
HD148387	G8IIIab	4.35	3.65	2.74	2.12	1.66	–	–	1.17	–	0.61	0.001	4826	71	–0.11	M03	PASTEL	1
HD027697	K0III	5.56	4.74	3.76	–	–	–	–	2.15	–	1.59	0.000	4826	51	0.09	B09	PASTEL	1
HD028305	G9.5III	5.42	4.54	3.53	–	–	–	–	1.90	–	1.32	0.000	4827	44	0.11	B09	PASTEL	1
HD150997	G7.5IIIbF	5.03	4.42	3.50	2.83	2.35	–	–	1.98	–	1.35	0.000	4841	63	–0.17	M03	PASTEL	1
HD028305	G9.5III	5.42	4.54	3.53	–	–	–	–	1.90	–	1.32	0.000	4843	62	0.11	M03	MILES	2
HD027371	K0III	5.46	4.64	3.65	–	–	–	–	2.02	–	1.49	0.000	4844	47	0.13	B09	PASTEL	1
HD135722	G8III	5.07	4.40	3.46	2.74	2.24	–	–	1.79	1.26	1.19	0.009	4850	60	–0.36	M03	PASTEL	1
HD180711	G9III	4.84	4.06	3.06	2.37	1.86	–	–	1.43	–	0.80	0.002	4851	67	–0.20	M03	PASTEL	1
HD062509	K0IIIb	3.00	2.14	1.14	0.39	–0.11	–	–	–0.52	–1.00	–1.11	0.000	4858	60	0.06	M03	PASTEL	1
HD027697	K0III	5.52	4.71	3.74	–	–	–	–	2.14	–	1.59	0.007	4897	65	0.09	M03	PASTEL	4
HD133208	G8IIIaBa0	5.10	4.38	3.45	2.80	2.34	–	–	1.88	1.42	1.33	0.022	5017	53	–0.05	M03&Ba10a	PASTEL	1
HD148856	G7IIIa	4.22	3.56	2.66	2.05	1.60	–	–	1.18	0.67	0.61	0.034	4979	61	–0.16	M03	PASTEL	1
HD113226	G8IIIab	4.45	3.71	2.79	2.16	1.71	–	–	1.29	0.77	0.80	0.000	4981	61	0.13	M03	PASTEL	1
HD202109	G8III/III	4.82	4.08	3.12	2.45	2.00	–	–	1.58	1.13	1.07	0.029	5002	62	–0.06	M03	PASTEL	1
HD216131	G8III	5.08	4.41	3.47	2.79	2.32	–	–	1.93	–	1.37	0.004	5084	51	–0.05	M03&Ba10a	PASTEL	1
HD181827	K0III	–	8.20	7.19	–	–	–	–	5.50 ^a	–	4.90 ^a	0.000	5039	66	0.14	H12	PASTEL	1
HD100407	G7III	5.17	4.47	3.54	2.84	2.36	3.06	2.63	2.04	1.57	1.45	0.000	5044	33	0.08	R13	PASTEL	1
HD189349	G5III	–	7.90	7.09	–	–	–	–	5.63 ^a	5.13 ^a	5.13 ^a	0.070	5282	72	–0.56	H12	H12	2
HD205435	G5III	5.47	4.91	4.02	3.31	2.81	–	–	2.47	2.06	1.96	0.000	5663	74	–0.13	Ba10a	PASTEL	1

Notes. Spectral types are taken from the SIMBAD database (<http://simbad.u-strasbg.fr/simbad/>) or from Ducati (2002).

Photometric magnitudes of the Johnson system ($UBVRJHK$) are taken from B12b, B13, Ducati (2002), Mermilliod et al. (1997) and from the Lausanne photometric data base (<http://obswww.unige.ch/gcpd/gcpd.html>).

Flag1 and Flag2 give respectively the references from which the value of T_{eff} and [Fe/H] is taken from.

The references are: N94–North et al. (1994); M03–Mozurkewich et al. (2003); W04–Wittkowski et al. (2004); MILES–Sánchez-Blázquez et al. (2006); W06–Wittkowski et al. (2006); N07–North et al. (2007); Ba08–Baines et al. (2008); Ba09–Baines et al. (2009); B09–Boyajian et al. (2009); Ba10a–Baines et al. (2010a); Ba10b–Baines et al. (2010b); PASTEL–Soubiran et al. (2010); Ba11–Baines et al. (2011); B12b–Boyajian et al. (2012b); C12–Cusano et al. (2012); H12–Huber et al. (2012); K12–Koleva & Vazdekis (2012); R13–Ruchti et al. (2013); B13–Boyajian et al. (2013); M13–Maestro et al. (2013).

Flag3 indicates the method used for the extinction determination. See Table 2 for details.

^a The Johnson JHK magnitudes are converted from the 2MASS photometry. See Section 2 for details.

^b Stars with angular diameters determined using the surface–brightness relations of Kervella et al. (2004).

* Stars with multiple direct effective temperature measurements. The adopted value is the mean weighted by the uncertainties of individual measurements.

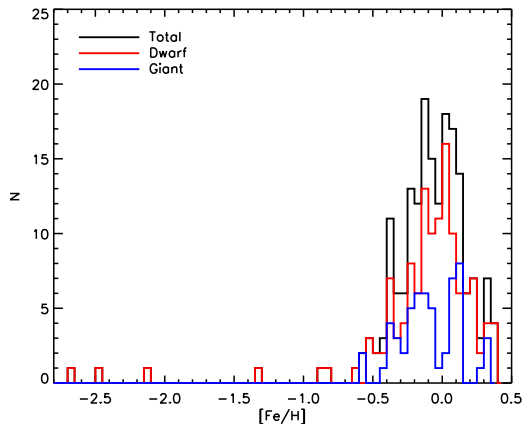


Figure 1. Metallicity distributions of our sample stars compiled from the literature. The black, red and blue histograms represent the distributions of the whole, the dwarf and the giant samples, respectively.

The metallicity $[\text{Fe}/\text{H}]$ of these stars are mainly taken from the PASTEL catalog (Soubiran et al. 2010), a bibliographical compilation of measurements of stellar atmospheric parameters (T_{eff} , $\log g$, $[\text{Fe}/\text{H}]$), mostly obtained from the analysis of high resolution ($R \geq 30,000$) and high signal-to-noise ratio ($S/N \geq 100$) spectra. As of the version of April, 2013, over 8000 stars catalogued by the PASTEL have at least one set of determinations for all the three parameters T_{eff} , $\log g$ and $[\text{Fe}/\text{H}]$. Amongst them, more than 3000 (36 per cent) stars have at least two independent determinations available for $[\text{Fe}/\text{H}]$. There are 166 stars (85 per cent) stars in our sample that have all three atmospheric parameters available from the PASTEL. For those stars with multiple $[\text{Fe}/\text{H}]$ determinations, we simply take the mean values with 3σ clipping. The $[\text{Fe}/\text{H}]$ values of the remaining 21 (11 per cent) stars are taken from the literature not included in PASTEL. There are still 8 (4 per cent) stars without a $[\text{Fe}/\text{H}]$ determination. The distributions of $[\text{Fe}/\text{H}]$ values of dwarfs and giants in our sample range from ~ -0.8 to 0.4 (Population I) except for a few metal-poor dwarfs as shown in Fig. 1.

Four photometric systems are used in the current work to derive the empirical metallicity-dependent T_{eff} -colour relations: the standard Johnson ($UBVR_I JHK$), the Cousins ($R_C I_C$), the SDSS (gr) and the 2MASS (JHK_s , hereafter J_2 , H_2 and K_2 in order to distinguish from the Johnson J , H and K). Most stars in our sample have high quality multiple measurements in the Johnson system, especially in B and V bands (the magnitudes of the two bands are available for all stars in our sample). Cousins ($R_C I_C$) magnitudes available for the current sample of stars are quite limited, especially for giants (about 10 stars). The J_2 , H_2 and K_2 magnitudes for most stars are saturated because they are too bright for 2MASS. For the same reason, there are no SDSS photometry for all sample stars. On the other hand, the later two photometric systems are of particular interest for the potential applications of the empirical relations discussed here, considering that 2MASS is one of the major near-infrared all sky survey that yields high precision photometry for nearly 471 million point-like sources (Skrutskie et al. 2006) and that the SDSS-like filters are now the most widely used in modern large-scale digital sky surveys including the Xuyi Schmidt Telescope Photometric Survey of the Galactic Anticentre (XSTPS-GAC; Zhang et al. 2013, 2014; Liu et al. 2014), the Panoramic Survey Telescope & Rapid Response System survey (PanSTARRS; Kaiser et al. 2002), the SkyMapper (Keller et

Table 2. Summary of $E(B - V)$ determinations

Flag	Method*	N_{star}
0	$d \leq 20$ pc, $A_V = 0$	3
1	'star pairs'	154
2	literature	12
3	SFD98	15
4	extinction-distance relation	11

* When the extinction of a star has been determined with multiple methods, we adopt the one with the highest priority. The priority, from high to low, is given by Flag value sequence 1, 2, 3, 4 and 0.

al. 2007) and the future Large Synoptic Survey Telescope survey (LSST; LSST collaboration 2009). It is thus essential to derive the empirical metallicity-dependent T_{eff} -colour relations in term of the SDSS and 2MASS photometric colours. In order to obtain magnitudes in the SDSS and 2MASS photometric systems, we have applied transformation equations that convert the Johnson magnitudes to those two systems for our sample stars. For the SDSS photometry system, g and r magnitudes are deduced from the Johnson B and V magnitudes using the transformations derived by Jester et al. (2005). For the 2MASS J_2 , H_2 and K_2 , we first convert the Johnson magnitudes to the system of Bessell & Brett using the transformations given by Bessell & Brett (1988) and then to the 2MASS system using the transformations of Carpenter (2001)². Only a few stars in our sample have Johnson J , H and K photometry unavailable, but instead have good 2MASS photometry³. For those stars, we obtain their Johnson J , H and K magnitudes from the 2MASS ones by reversing the aforementioned transformations.

Accurate reddening corrections are essential for constructing robust metallicity-dependent T_{eff} -colour empirical relations, particularly for giant stars, which suffer from relatively high extinction given their large distances. For most of the sample stars, we have adopted extinction values deduced from the photometric colours using the 'standard pair' technique (Stecher 1965; Massa et al. 1983; Yuan et al. 2013). The technique assumes that stars of similar atmospheric parameters (T_{eff} , $\log g$, $[\text{Fe}/\text{H}]$) should have similar colours. For this purpose, we first define a 'reference library' by selecting stars with nil/low extinction and with all the three atmospheric parameters available from the PASTEL catalog. Then the extinction values of the current sample stars are estimated by comparing their observed colours with those in the 'reference library' that have similar atmospheric parameters. A comparison with values given by the integrated extinction map of Schlegel, Finkbeiner & Davis (1998, hereafter SFD98) for high Galactic latitude stars shows the technique has achieved a precision of about 0.02 mag in $E(B - V)$. The reddening values of $E(B - V)$ for 154 (79 per cent) sample stars are estimated with this method. For the remaining stars, reddening values are adopted either from the literature, from the SFD98 map for stars of high Galactic latitudes, from extinction-distance relation that we derive for that particular line-of-sight⁴, or simply set to zero when they are close (within 20 pc).

² We adopt the latest transformations available from <http://www.astro.caltech.edu/~jmc/2mass/v3/transformations/>.

³ Only stars with *ph_qual* flag flagged 'A' and photometric error less than 0.05 mag in all three 2MASS bands are considered as having good photometry.

⁴ We first determine the extinction values for all stars in the PASTEL catalog that have all the three atmospheric parameters available. Then

Table 3. Fit coefficients, applicability ranges in metallicity and colour of the metallicity-dependent T_{eff} -colour relations for dwarfs

Colour	[Fe/H] range	Colour range	a_0	a_1	a_2	a_3	a_4	a_5	N	s.d.(%)	Type
$U - V$	[-0.8, 0.4]	[+0.11, 2.58]	0.64612	0.32629	-0.05032	-0.02288	-0.14090	-0.04187	42	2.18	AFGKM
$U - V$	[-0.8, 0.4]	[+0.16, 2.58]	0.68567	0.25708	-0.02644	-0.03637	-0.09993	-0.03003	40	1.73	FGKM
$B - V$	[-0.9, 0.4]	[-0.05, 1.73]	0.59225	0.39926	0.07848	-0.04374	-0.04289	-0.01406	120	2.02	AFGKM
$B - V$	[-0.9, 0.4]	[+0.32, 1.73]	0.63421	0.30538	0.12308	-0.06216	-0.01987	-0.00951	111	1.96	FGKM
$V - R_J$	[-0.9, 0.4]	[-0.04, 1.69]	0.53767	0.66928	-0.05870	-0.04605	-0.02025	-0.01402	86	3.21	AFGKM
$V - R_J$	[-0.9, 0.4]	[+0.32, 1.69]	0.50741	0.74628	-0.10012	-0.05966	-0.00411	-0.00297	71	2.64	FGKM
$R_J - I_J$	[-0.9, 0.4]	[-0.03, 1.43]	0.55253	1.09402	-0.32146	-0.12854	0.03871	-0.00030	84	2.89	AFGKM
$R_J - I_J$	[-0.9, 0.4]	[+0.18, 1.43]	0.52917	1.18647	-0.38691	-0.14505	0.05246	0.00312	73	2.73	FGKM
$V - I_J$	[-0.9, 0.4]	[-0.07, 3.12]	0.54700	0.41277	-0.03462	-0.04607	0.00706	-0.01032	86	2.79	AFGKM
$V - I_J$	[-0.9, 0.4]	[+0.51, 3.12]	0.50673	0.47658	-0.05391	-0.04491	0.01236	-0.00734	73	2.43	FGKM
$V - R_C$	[-0.8, 0.3]	[-0.05, 1.21]	0.56180	0.93029	-0.11466	-0.15858	0.02426	-0.00998	41	2.51	AFGKM
$V - R_C$	[-0.8, 0.2]	[+0.22, 1.21]	0.57684	0.87545	-0.07718	-0.22472	0.06639	-0.00347	33	2.35	FGKM
$R_C - I_C$	[-0.8, 0.3]	[-0.01, 1.56]	0.53569	1.17516	-0.36436	-0.24823	0.05024	-0.02187	41	2.93	AFGKM
$R_C - I_C$	[-0.8, 0.2]	[+0.22, 1.56]	0.52327	1.22375	-0.39607	-0.30792	0.08613	-0.01724	35	2.69	FGKM
$V - I_C$	[-0.8, 0.3]	[-0.06, 2.77]	0.54447	0.54119	-0.06920	-0.10748	0.04723	-0.01367	40	2.46	AFGKM
$V - I_C$	[-0.8, 0.2]	[+0.44, 2.77]	0.53066	0.56556	-0.07742	-0.13244	0.07752	-0.00969	34	2.38	FGKM
$V - J$	[-0.9, 0.4]	[-0.12, 4.24]	0.54007	0.33983	-0.02512	-0.05359	0.06601	-0.00133	107	2.28	AFGKM
$V - J$	[-0.9, 0.4]	[+0.60, 4.24]	0.51683	0.36567	-0.03065	-0.05507	0.06928	-0.00047	95	2.08	FGKM
$V - H$	[-0.9, 0.4]	[-0.13, 4.76]	0.55015	0.24801	-0.00887	-0.04204	0.06782	-0.00168	103	2.31	AFGKM
$V - H$	[-0.9, 0.4]	[+0.67, 4.76]	0.57826	0.22238	-0.00473	-0.07342	0.13820	0.01264	92	2.00	FGKM
$V - K$	[-0.9, 0.4]	[-0.15, 5.03]	0.55261	0.23293	-0.00757	-0.03760	0.05030	-0.00516	107	1.96	AFGKM
$V - K$	[-0.9, 0.4]	[+0.82, 5.03]	0.56784	0.22038	-0.00585	-0.06218	0.10765	0.00651	97	1.87	FGKM
$g - r$	[-0.9, 0.4]	[-0.28, 1.53]	0.68692	0.42617	0.07504	-0.04372	-0.05220	-0.01390	120	2.02	AFGKM
$g - r$	[-0.9, 0.4]	[+0.10, 1.53]	0.70726	0.33962	0.13127	-0.04405	-0.03616	-0.00935	109	1.86	FGKM
$g - J$	[-0.9, 0.4]	[-0.24, 5.15]	0.57513	0.24031	-0.01020	-0.03323	0.03011	-0.00494	108	2.06	AFGKM
$g - J$	[-0.9, 0.4]	[+0.67, 5.15]	0.56499	0.24982	-0.01194	-0.03654	0.03880	-0.00298	95	1.88	FGKM
$g - H$	[-0.9, 0.4]	[-0.25, 5.68]	0.57538	0.19009	-0.00388	-0.02659	0.03663	-0.00357	102	2.11	AFGKM
$g - H$	[-0.9, 0.4]	[+0.75, 5.68]	0.60421	0.16755	-0.00064	-0.05271	0.10246	0.00965	93	1.93	FGKM
$g - K$	[-0.9, 0.4]	[-0.27, 5.95]	0.57596	0.18108	-0.00342	-0.02443	0.02469	-0.00617	107	1.90	AFGKM
$g - K$	[-0.9, 0.4]	[+0.89, 5.95]	0.59712	0.16510	-0.00123	-0.04565	0.07963	0.00481	96	1.76	FGKM
$V - J_2$	[-0.9, 0.4]	[-0.06, 4.28]	0.52082	0.34241	-0.02495	-0.05376	0.06846	-0.00170	107	2.26	AFGKM
$V - J_2$	[-0.9, 0.4]	[+0.66, 4.28]	0.49543	0.36971	-0.03068	-0.05506	0.07191	-0.00066	95	2.07	FGKM
$V - H_2$	[-0.9, 0.4]	[-0.13, 4.77]	0.54872	0.24869	-0.00896	-0.04212	0.06615	-0.00232	103	2.25	AFGKM
$V - H_2$	[-0.9, 0.4]	[+0.69, 4.77]	0.57565	0.22418	-0.00501	-0.07282	0.13574	0.01211	92	1.95	FGKM
$V - K_2$	[-0.9, 0.4]	[-0.10, 5.05]	0.54042	0.23676	-0.00796	-0.03798	0.05413	-0.00448	113	1.98	AFGKM
$V - K_2$	[-0.9, 0.4]	[+0.86, 5.05]	0.55470	0.22536	-0.00647	-0.06318	0.11273	0.00697	103	1.88	FGKM
$g - J_2$	[-0.9, 0.4]	[-0.18, 5.19]	0.56153	0.24125	-0.01009	-0.03327	0.03191	-0.00499	108	2.05	AFGKM
$g - J_2$	[-0.9, 0.4]	[+0.73, 5.19]	0.55158	0.25030	-0.01172	-0.03662	0.04096	-0.00296	95	1.87	FGKM
$g - H_2$	[-0.9, 0.4]	[-0.25, 5.68]	0.57407	0.19046	-0.00390	-0.02663	0.03644	-0.00342	101	2.02	AFGKM
$g - H_2$	[-0.9, 0.4]	[+0.77, 5.68]	0.60082	0.16907	-0.00078	-0.04698	0.07517	0.00001	91	1.77	FGKM
$g - K_2$	[-0.9, 0.4]	[-0.22, 5.96]	0.56653	0.18358	-0.00365	-0.02477	0.02794	-0.00552	113	1.91	AFGKM
$g - K_2$	[-0.9, 0.4]	[+0.94, 5.96]	0.58681	0.16856	-0.00163	-0.04666	0.08483	0.00564	102	1.79	FGKM

Table 4. Fit coefficients, applicability ranges in metallicity and colour of the metallicity-dependent T_{eff} -colour relations for giants

Colour	[Fe/H] range	Colour range	a_0	a_1	a_2	a_3	a_4	a_5	N	s.d.(%)	Type
$U - V$	[-0.6, 0.3]	[1.53, 3.55]	0.85926	0.06128	0.02054	0.00341	-0.04250	0.08760	45	1.55	GKM
$B - V$	[-0.6, 0.3]	[0.88, 1.59]	0.81784	0.03096	0.19350	-0.03292	0.00762	0.11140	51	1.86	GKM
$V - R_J$	[-0.6, 0.3]	[0.61, 2.05]	0.50982	0.86731	-0.16385	0.00099	-0.05206	-0.03531	39	2.14	GKM
$R - I_J$	[-0.6, 0.3]	[0.45, 1.91]	0.58534	1.07395	-0.30028	0.08547	-0.07481	0.10417	39	2.34	GKM
$V - I_J$	[-0.6, 0.3]	[1.06, 3.96]	0.51361	0.51406	-0.06282	0.03408	-0.09130	0.01118	39	1.96	GKM
$V - J$	[-0.6, 0.3]	[1.45, 4.90]	0.46448	0.42236	-0.03986	-0.01037	0.00000	-0.06615	48	1.92	GKM
$V - H$	[-0.6, 0.3]	[1.95, 5.80]	0.42078	0.33924	-0.02323	-0.04718	0.11736	-0.05597	23	0.93	GKM
$V - K$	[-0.6, 0.3]	[1.96, 6.08]	0.47934	0.29738	-0.01888	-0.02526	0.06059	-0.04110	48	1.68	GKM
$g - r$	[-0.6, 0.3]	[0.66, 1.39]	0.82134	0.14378	0.17360	-0.02994	-0.00477	0.10091	51	1.88	GKM
$g - J$	[-0.6, 0.3]	[1.81, 5.73]	0.49851	0.30054	-0.01921	-0.01956	0.02561	-0.04232	48	1.72	GKM
$g - H$	[-0.6, 0.3]	[2.31, 6.63]	0.46461	0.25124	-0.01189	-0.03594	0.09960	-0.03641	23	0.93	GKM
$g - K$	[-0.6, 0.3]	[2.32, 6.91]	0.51612	0.22256	-0.00966	-0.01988	0.04938	-0.03274	48	1.59	GKM
$V - J_2$	[-0.6, 0.3]	[1.51, 4.95]	0.44863	0.41980	-0.03858	-0.02540	0.03704	-0.05304	48	1.90	GKM
$V - H_2$	[-0.6, 0.3]	[1.94, 5.79]	0.42367	0.33746	-0.02298	-0.04768	0.11713	-0.05342	23	0.92	GKM
$V - K_2$	[-0.6, 0.3]	[1.99, 6.09]	0.46447	0.30156	-0.01918	-0.02526	0.06132	-0.04036	48	1.68	GKM
$g - J_2$	[-0.6, 0.3]	[1.87, 5.78]	0.47230	0.30872	-0.02003	-0.01081	-0.00000	-0.05341	48	1.72	GKM
$g - H_2$	[-0.6, 0.3]	[2.30, 6.63]	0.46683	0.25008	-0.01175	-0.03545	0.09634	-0.03581	23	0.93	GKM
$g - K_2$	[-0.6, 0.3]	[2.35, 6.92]	0.50481	0.22511	-0.00980	-0.01982	0.04878	-0.03720	48	1.59	GKM

Table 2 presents a summary of the number of stars with their extinction determined by each method. Finally, we correct the measured photometric magnitudes of each band for the interstellar reddening

using the above estimated values of $E(B - V)$ and the extinction law of Fitzpatrick (1999) for $R = 3.1$.

All relevant information of our sample compiled here, including T_{eff} , photometric magnitudes⁵ after reddening corrections, ex-

we construct a library consisting of stars that have extinction determinations and geometric distances from the Hipparcos (van Leeuwen 2007). An extinction-distance relation is then constructed using the stars in the library that fall within a solid angle (typically 4 square degree) of line-of-sight to a sample star of concern here.

⁵ Magnitudes converted from photometric measurements in other bands, i.e. those of SDSS g, r and 2MASS $J_2H_2K_2$, are not listed in the Table. One can obtain their values using the transformations described in Section 2.

tion, [Fe/H] and etc., is presented in Table 1. Unless specified otherwise, all magnitudes and colours presented in the paper refer to dereddened values.

3 EMPIRICAL CALIBRATIONS

To obtain the metallicity-dependent T_{eff} -colour relations, data for dwarf and giant stars are fitted separately following the conventional approach (e.g. Alonso et al. 1996, 1999; Ramírez & Meléndez 2005; Casagrande et al. 2006; González Hernández & Bonifacio 2009; Casagrande et al. 2010):

$$\theta_{\text{eff}} = a_0 + a_1X + a_2X^2 + a_3X[\text{Fe}/\text{H}] + a_4[\text{Fe}/\text{H}] + a_5[\text{Fe}/\text{H}]^2, \quad (1)$$

where $\theta_{\text{eff}} = 5040/T_{\text{eff}}$, X represents the colour of concern and a_i ($i = 0, \dots, 5$) are the fit coefficients. We iterate the fitting, discarding data points that deviate more than 2.5σ from the fit. In general, three to four iterations are sufficient.

The polynomial fits to the empirical relations are shown for dwarf stars in Figs. 2–5 and giants in Figs. 6–8. The fit coefficients (a_i) for eighteen colours are given in Table 3 for dwarfs and Table 4 for giants, along with the standard deviation (s.d.), of the percentage errors of the fit, i.e. $(T_{\text{eff}}^{\text{fit}} - T_{\text{eff}})/T_{\text{eff}} \times 100$, the number of stars used for the final fit (after the 2.5σ clipping) N , the applicability ranges of the fit in colour and [Fe/H], and finally the spectral types corresponding to the colour range. The fits for dwarf stars are performed for the full range of AFGKM stars. However, as indicated by some recent studies (Monnier et al. 2007; van Belle 2012; B13), there may exist biases in the determinations of T_{eff} by interferometric imaging for stars earlier than mid-F due to their rapid rotation. Following B13, we have thus provided another set of fits, excluding stars hotter than 6750 K. The results are also given in Table 3 with the corresponding range of spectral type marked as FGKM. For all the twenty-one colours, the maximum differences between the temperature given by the T_{eff} -colour relations⁶ with and without early-type stars are all within a few percent (0.6–1.5 per cent). As mentioned earlier, the number of giant stars with the Cousins $R_C I_C$ magnitudes available is too small (~ 10) to fit the empirical metallicity-dependent T_{eff} -colour relations. Thus we only consider the Cousins $R_C I_C$ system in the calibrations for dwarfs. The standard deviations of the percentage residuals of the fit are about 2.0 and 1.5 per cent for dwarfs and giants, respectively.

Finally, we note that our sample includes four dwarfs (nicely sample FGK star covering a wide range of T_{eff} from $\sim 4,600$ to 6,300 K) of metallicities [Fe/H] ~ -2.0 , which provide some constraints on the relations at such low metallicities. Applying the relations to such low metallicities should be however treated with caution.

3.1 Metallicity effects

The intrinsic colours of a star are not only governed by T_{eff} but also by metallicity due to the line blanketing effects (e.g. Ramírez and Meléndez 2005, hereafter RM05). As shown in Figs. 2–5, the effects of metallicity on the T_{eff} versus colour relations for dwarf stars show two distinct features. Firstly, colours involving bands in the UV and optical (e.g. $U - V$, $B - V$, $V - R_1/R_C$, $g - r$) always get redder (larger) with increasing metallicity at a given T_{eff} . On the

other hand, for colours between a visual and a near-infrared band (e.g. $V - J/H/K$, $V - J_2/H_2/K_2$, $g - J/H/K$, $g - J_2/H_2/K_2$), while they get redder (larger) with increasing metallicity for cool stars (e.g. $T_{\text{eff}} < 6000$ K) for a given effective temperature, they actually become bluer (smaller) for hot stars (e.g. $T_{\text{eff}} > 6000$ K). These behaviors are similar to those found by calibrations based on the IRFM T_{eff} scale and have been explained in detail by RM05 using synthetic spectra.

Colour ($V - K$) (here K can be either of the Johnson or the 2MASS system; also as shown in Figs. 5 and 8, g is very similar to V) is often considered the best T_{eff} indicator (e.g. Blackwell et al. 1990; Alonso et al. 1996, 1999; RM05), owing to its relatively weak dependence on metallicity and luminosity (see the next Section). To investigate how well the colours between a visual (i.e. V or g) and an infrared (i.e. K or K_2) band serve as a T_{eff} indicator without considering the metallicity effects, we explore in Fig. 9 the relative errors that would be introduced in T_{eff} deduced from colour ($V - K_2$) or ($g - K_2$) for a dwarf of solar metallicity, if an incorrect metallicity has been assumed. The plot shows that if one can accept a T_{eff} error of 3.0 per cent, then ($V - K_2$) or ($g - K_2$) is good enough even simply assuming solar metallicity without considering the metallicity effects, for disk stars ([Fe/H] > -0.8) of T_{eff} between 4,500 and 6,900 K in the case of ($V - K_2$) and between 4,650 to 7,950 K in the case of ($g - K_2$). If one extrapolates and applies the current calibrations for metal-poor halo stars ([Fe/H] ~ -2.0), the corresponding usable range will be narrowed down to 5,000 – 6,000 K and to 5,300 – 6,500 K, for colours ($V - K_2$) and ($g - K_2$), respectively. The effects of metallicity on colours are shown in the lower panel of Fig. 9. On the whole, the changes in colours due to the metallicity effects are similar to those found for effective temperature. For the temperature range 5,000 $< T_{\text{eff}} < 7,000$ K, the effects on colours ($V - K_2$) and ($g - K_2$) for disk-like dwarfs ([Fe/H] > -0.8) are smaller than 0.07 mag, comparable to the typical colour measurement uncertainties (assuming a photometric error of 0.05 mag in each band). For halo dwarfs ([Fe/H] ~ -2.0), the effects are bigger as one expects. In summary, we conclude that colour ($V - K_2$) or ($g - K_2$) can be a robust, metallicity-independent T_{eff} estimator for disk dwarfs ([Fe/H] > -0.8) of temperatures 5,000 $\lesssim T_{\text{eff}} \lesssim 7,000$ K. However, for halo dwarfs ([Fe/H] ~ -2.0), those two colours only work well for a restricted temperature range, 5,000 $\lesssim T_{\text{eff}} \lesssim 6,000$ K, if one ignores the metallicity effects.

For giants, the metallicity effects are insignificant either for ($V - K_2$) or ($g - K_2$), owing to the relative narrow range of metallicity and effective temperature covered by the current sample. According to the results of RM05 based on the IRFM T_{eff} scale, the effects are similar to those of dwarf stars.

3.2 Luminosity (surface gravity) effects

The effects of luminosity (i.e. the surface gravity $\log g$) on effective temperature and colours are illustrated in Fig. 10. Colours ($V - K_2$) and ($g - K_2$) are insensitive to the luminosity effects in estimating T_{eff} for the whole parameter range of giants calibrated here if one accepts a 3.0 per cent uncertainty of determination. This is particularly true for colour ($g - K_2$), for which the luminosity effects are smaller or comparable to typical photometric uncertainties for stars in the temperature range 3,650 $< T_{\text{eff}} < 5,200$ K (the upper temperature limit for the calibration of giants).

We conclude that colour ($g - K_2$) can serve as an excellent effective temperature indicator for the currently on-going large scale stellar spectroscopic surveys, not only because of its weak de-

⁶ For a metallicity [Fe/H] of -0.1 , the typical value of the dwarf sample.

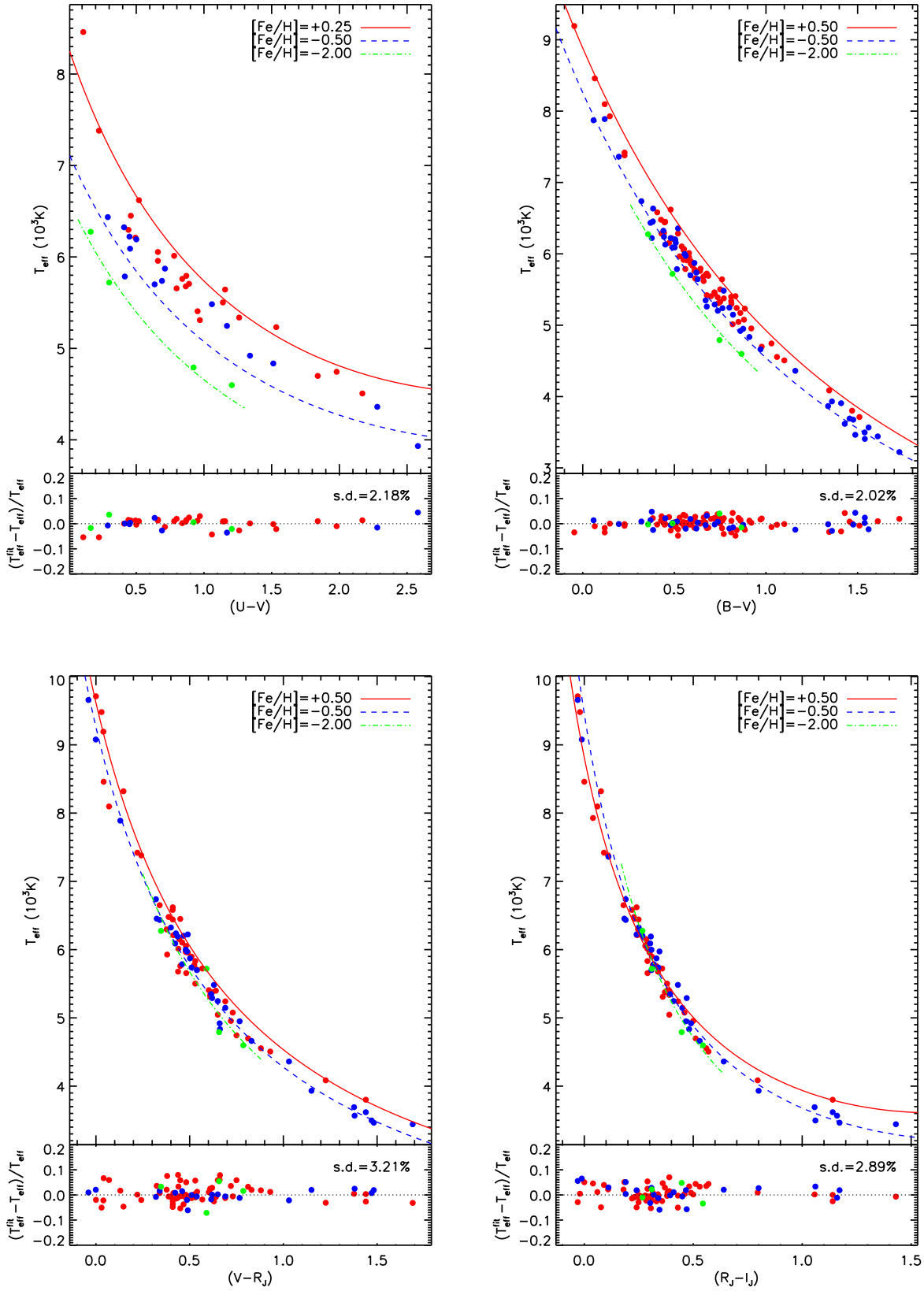


Figure 2. T_{eff} plotted against colours $U - V$, $B - V$, $V - R_J$ and $R_J - I_J$ for the dwarf sample in the metallicity bins $-0.1 < [\text{Fe}/\text{H}] < 0.5$ (red dots), $-1.0 < [\text{Fe}/\text{H}] \leq -0.1$ (blue dots) and $[\text{Fe}/\text{H}] \leq -1.0$ (green dots). The lines represent our best fits for selected values of $[\text{Fe}/\text{H}]$ as marked in each panel. The lower part of each panel shows the relative residuals of the fit $(T_{\text{eff}}^{\text{fit}} - T_{\text{eff}}) / T_{\text{eff}}$ as a function of colour.

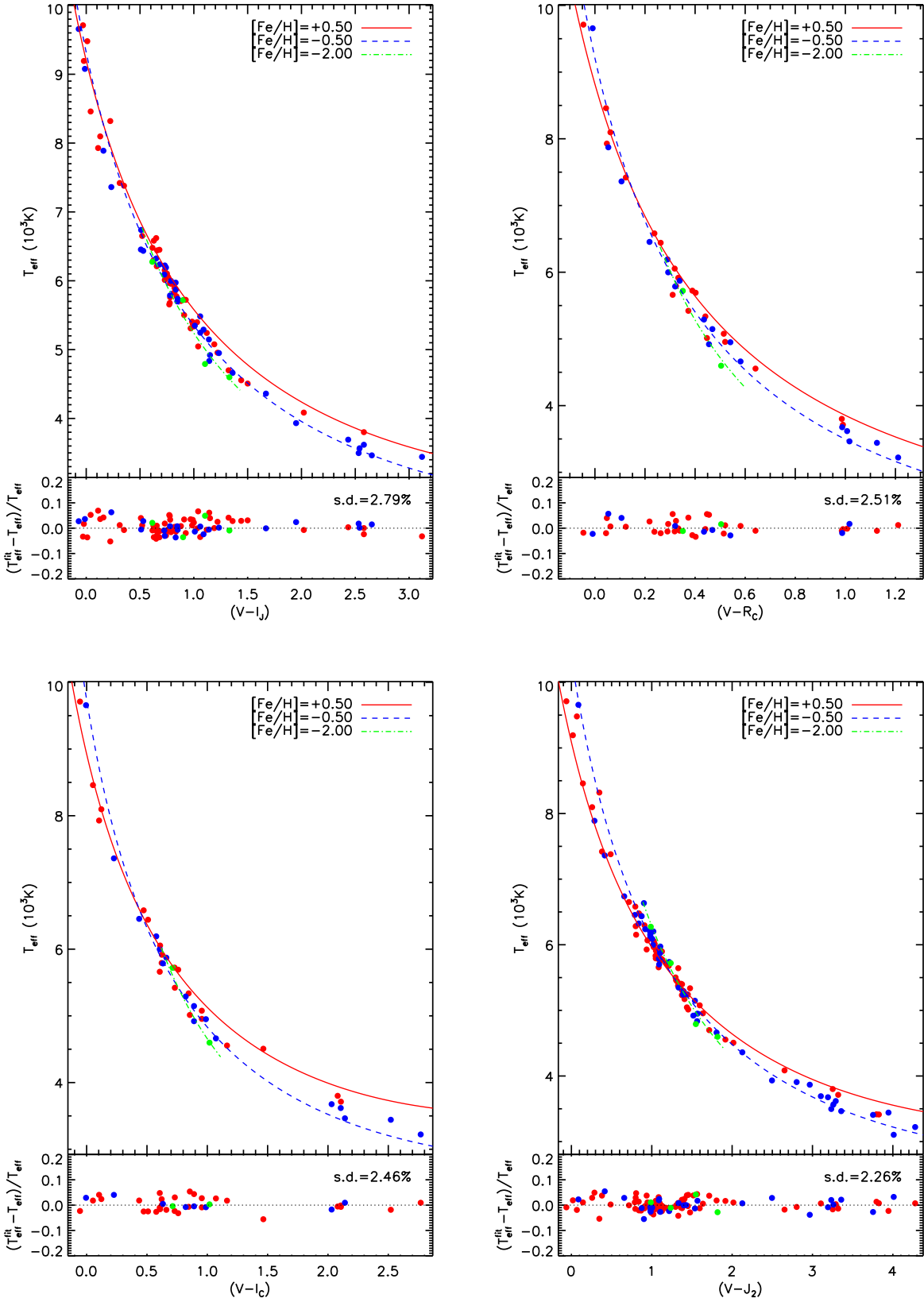


Figure 3. Same as Fig. 2 colours but for $V - I_J$, $V - R_C$, $V - I_C$ and $V - J_2$.

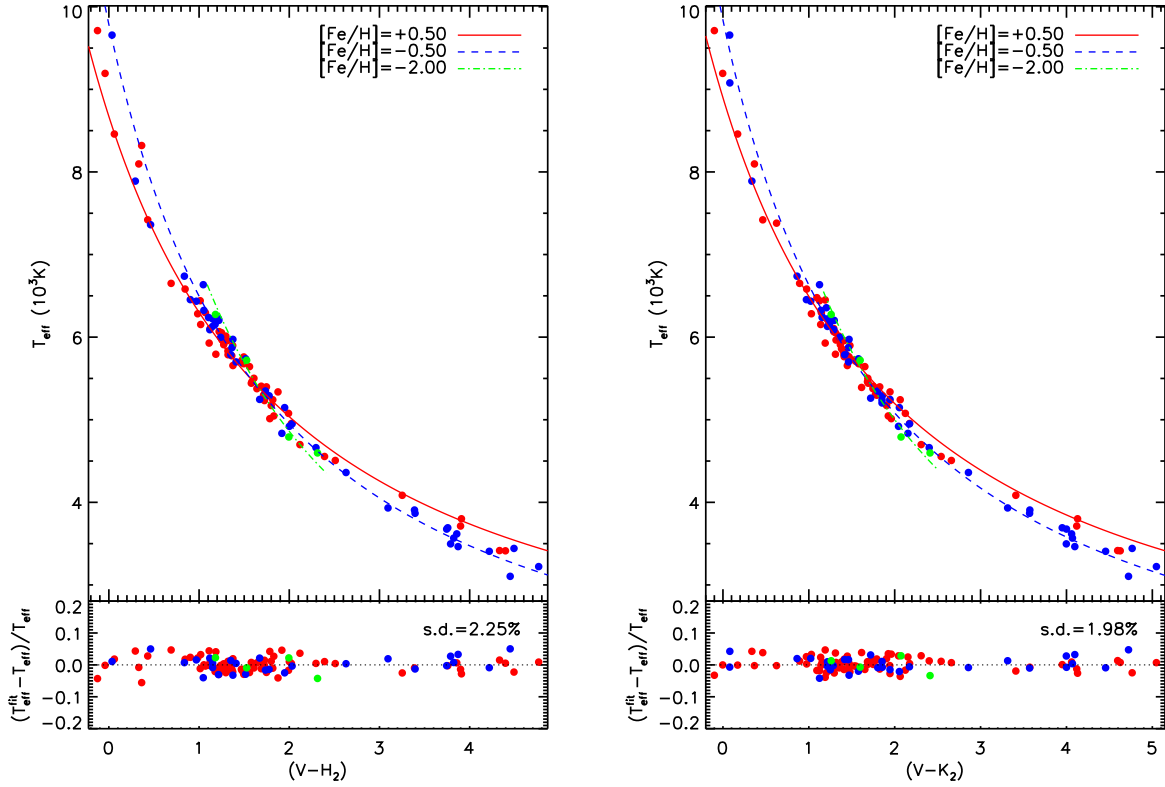


Figure 4. Same as Fig. 2 colours but for $V - H_2$ and $V - K_2$.

pendence on metallicity and luminosity but also because it is easily available from high precision photometric surveys such as the SDSS, XSTPS-GAC, PanSTARRS and 2MASS.

4 COMPARISONS WITH OTHER TEMPERATURE SCALES

In this section, the direct T_{eff} scale from the interferometry is compared to other T_{eff} scales from a variety of techniques, including that based on the IRFM (Alonso 1996, 1999; RM05; Casagrande et al. 2011), on the line depth ratios (Kovtyukh et al. 2003, 2004, 2006, 2007), on the excitation equilibrium of iron lines (Santos et al. 2004) and that based on fitting with synthetic spectra (Valenti & Fischer 2005). We present the mean temperature difference, ΔT_{eff} for objects analyzed by those alternative techniques that are in common with the current sample with direct temperature measurements from interferometry along with the standard deviation of the mean, s.d., and the number of common objects N in Table 5. The actual data points used for the comparisons are also presented in Fig. 11.

4.1 IRFM effective temperatures

The IRFM effective temperatures of Alonso et al. (1996, 1999) and RM05 do not deviate significantly from the direct measurements, as Table 5 and Fig. 11 show. For dwarfs the values of Alonso et al. (1996) and RM05 are slightly hotter than direct measurements. The average difference and standard deviation are $\Delta T_{\text{eff}} = 41$ K and s.d. = 129 K for Alonso et al. (1996) ($N = 39$), and $\Delta T_{\text{eff}} = 57$ K

and s.d. = 135 K for RM05 ($N = 54$). For giants, the agreement is excellent for both Alonso et al. (1996) and RM05, with average difference of just few tens Kelvin and standard deviations smaller than 80 K. Note that in the above comparisons, stars of $T_{\text{eff}} \leq 4,000$ K have been excluded, because the IRFM does not work well for stars cooler than ~ 4000 K. Nevertheless, those cool stars are also plotted in Fig. 11 for completeness. In general, for those stars the IRFM temperatures deviate somewhat from the direct measurements.

However, the effective temperatures of dwarfs of Casagrande et al. (2011)⁷ based on the IRFM or T_{eff} -colour relations calibrated by the IRFM are significant hotter than direct measurements⁸. As Table 5 and Fig. 11 show, the average difference amounts to $\Delta T_{\text{eff}} = 131$ K, with a standard deviation s.d. = 127 K ($N = 69$). The difference is significant that the IRFM temperature scale of Casagrande et al. (2011) may be too hot.

As discussed in previous work (e.g. Casagrande et al. 2006, 2010), the systematic differences seen in IRFM effective temperature scales given by different studies are mainly due to the different zero points adopted. Now with many stars available in the CALSPEC database⁹ that have spectrophotometric fluxes between 0.3 – 2.5 μm accurate to better than 1 – 2 per cent (Bohlin 2010), the calibration of the zero-point of IRFM effective temperature scale can be much improved. Alternatively, one can also renormalize the

⁷ The IRFM technique employed in Casagrande et al. (2011) is developed by Casagrande et al. (2010).

⁸ For giants, there is no common sources between the two samples.

⁹ <http://www.stsci.edu/hst/observatory/cdbs/calspec.html/>

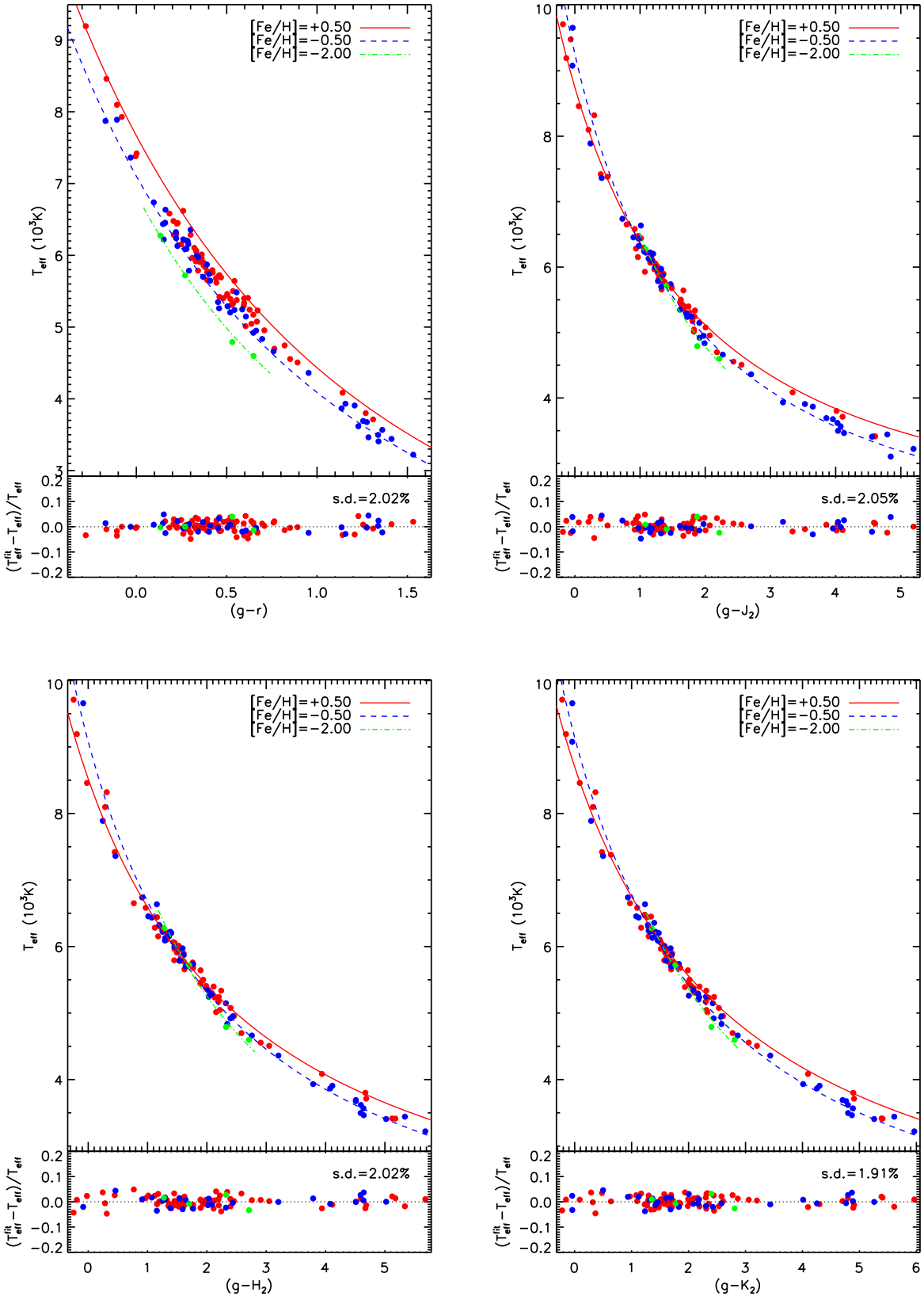


Figure 5. Same as Fig. 2 colours but for $g-r$, $g-J_2$, $g-H_2$ and $g-K_2$.

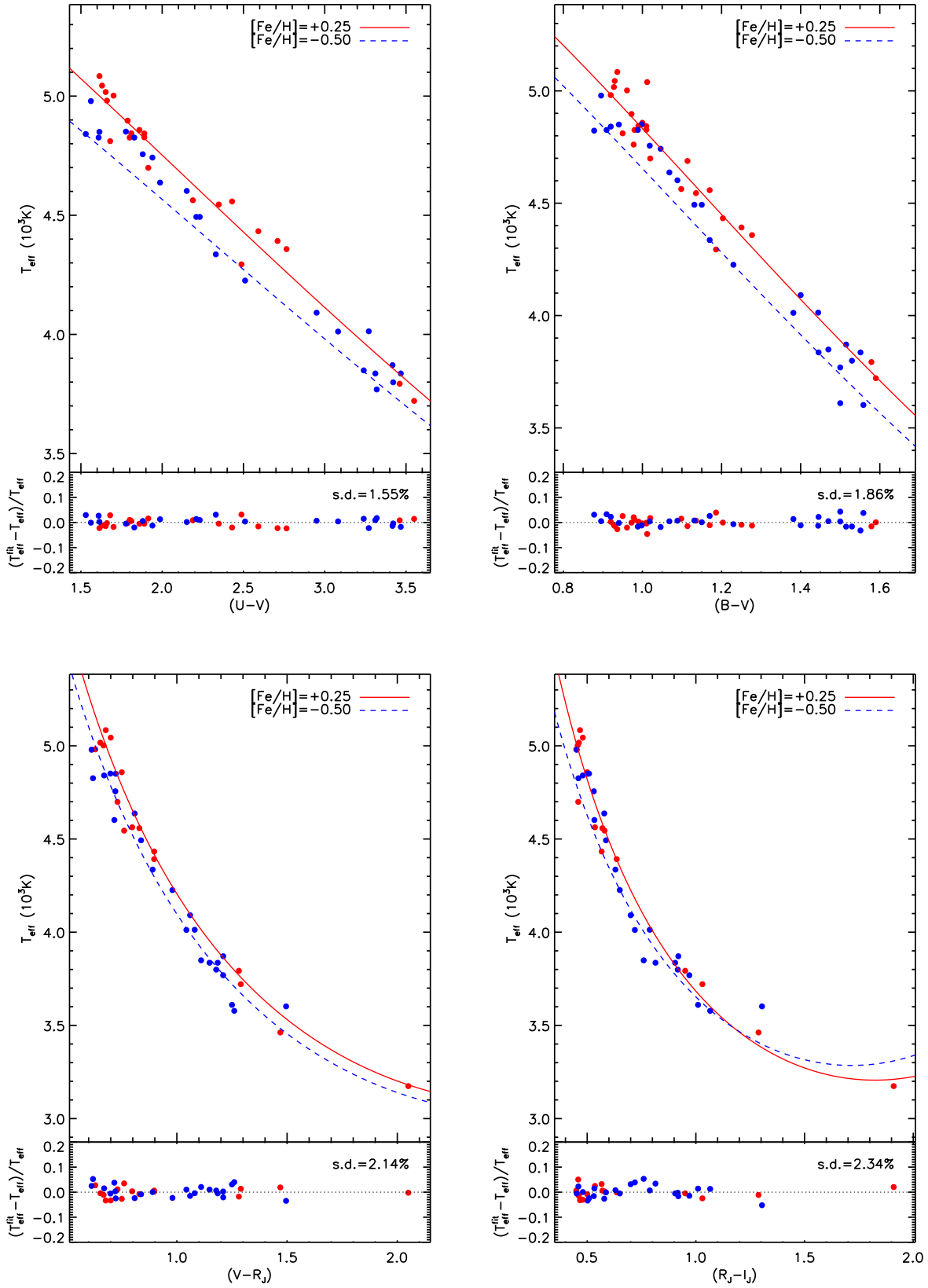


Figure 6. Same as Fig. 2 but for the sample of giants. Red and blue dots represent data points the metallicity bins $-0.1 < [\text{Fe}/\text{H}] < 0.5$ and $[\text{Fe}/\text{H}] \leq -0.1$, respectively.

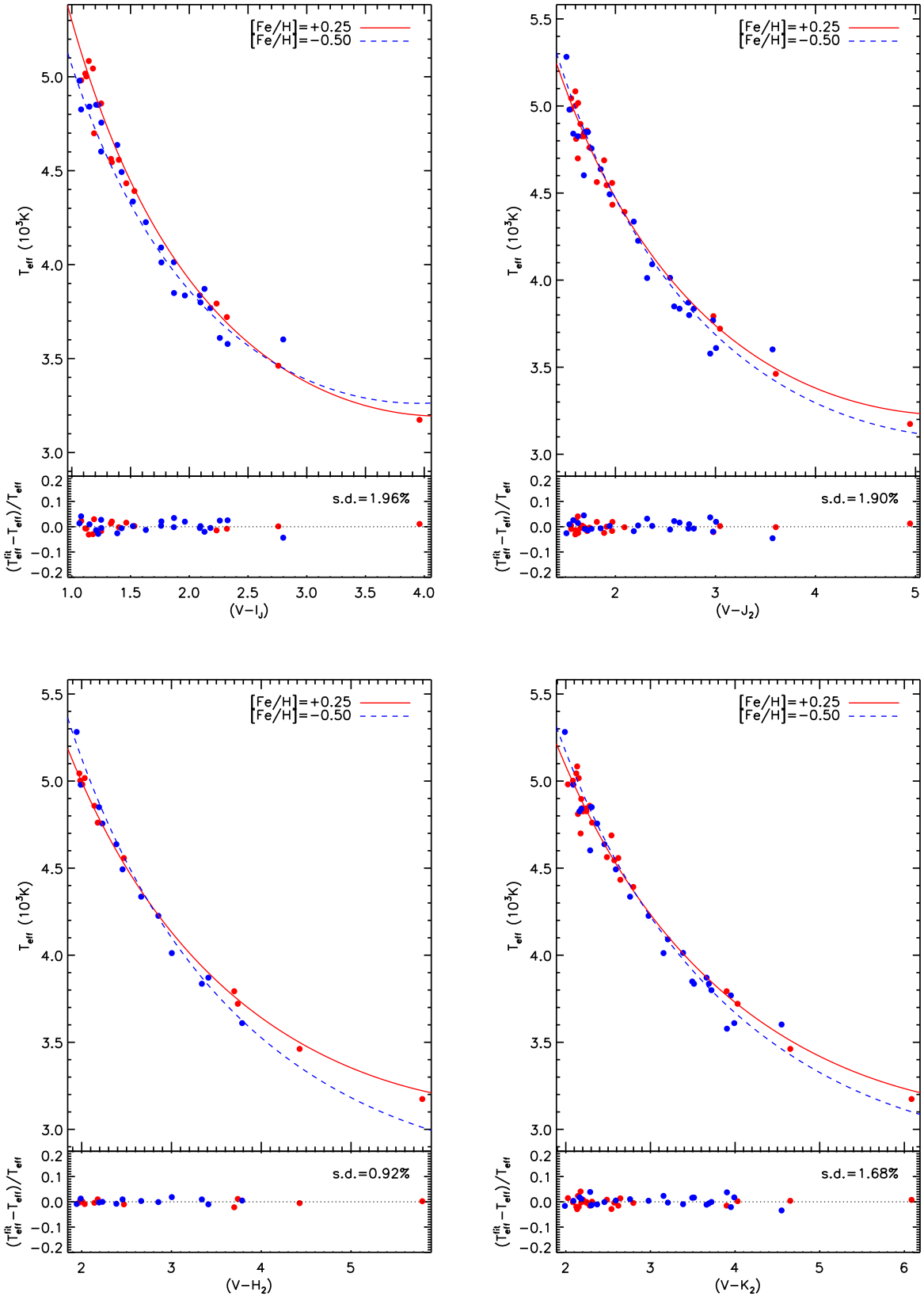


Figure 7. Same as Fig. 6, but for colours $V - I_J$, $V - J_2$, $V - H_2$ and $V - K_2$.

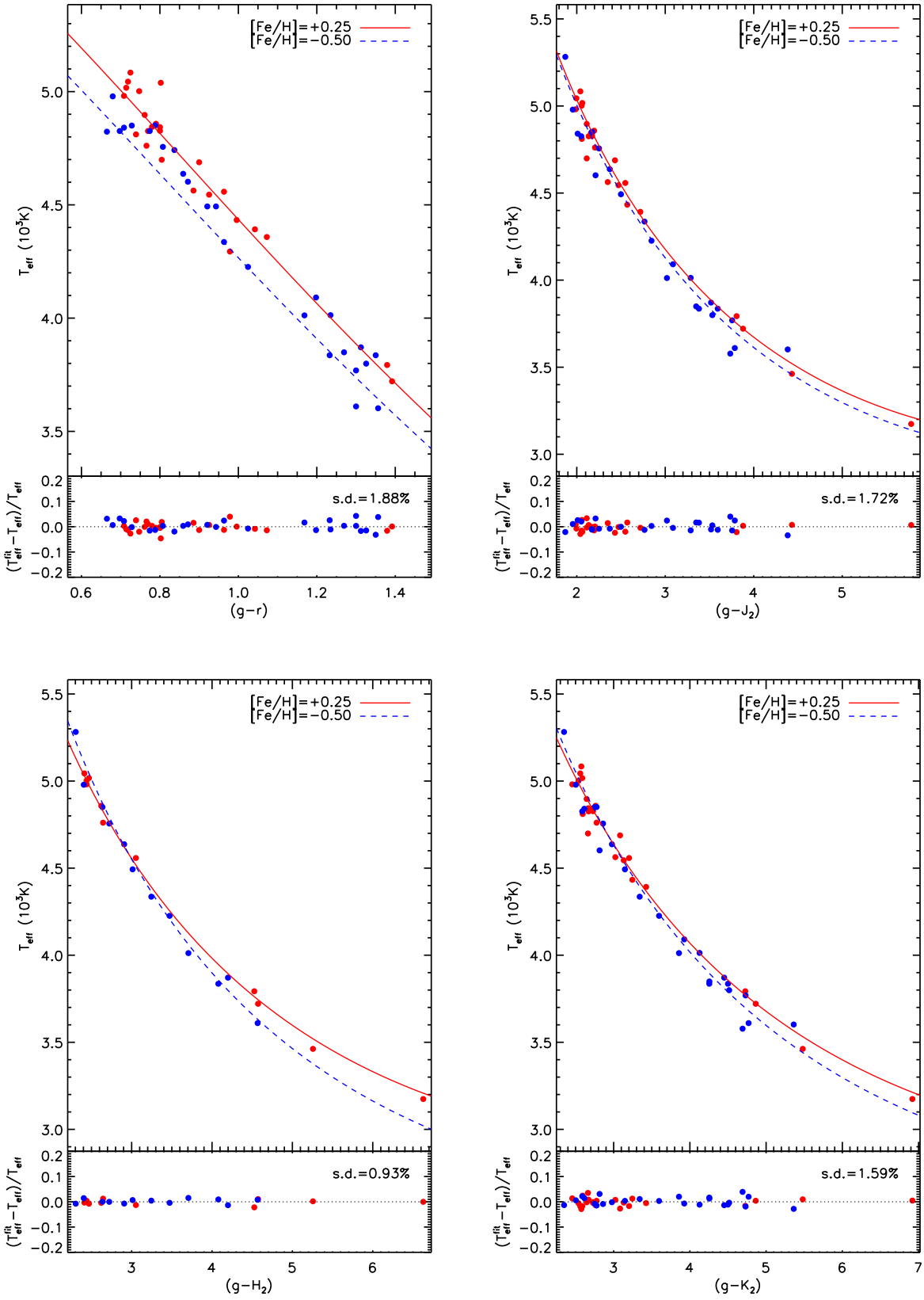


Figure 8. Same as Fig. 6, but for colours $g-r$, $g-J_2$, $g-H_2$ and $g-K_2$.

Table 5. Comparisons with other effective temperature scales

Source	ΔT_{eff} (K)	s.d. (K)	N	Method
Dwarf stars				
Alonso et al. (1996)	41	139	39	IRFM
Santos et al. (2004)	127	129	24	Excitation equilibrium of Fe I lines
RM05	59	136	54	IRFM
Valentin & Fischer (2005)	91	118	59	Fitting with synthetic spectra
Kovtyukh et al. (2003, 2004)	57	94	36	Line-depth ratios
Casagrande et al. (2011)	131	127	69	IRFM or T_{eff} -colour relations*
Giant stars				
Alonso et al. (1999)	-4	77	15	IRFM
RM05	-16	76	14	IRFM
Kovtyukh et al. (2006, 2007)	82	89	14	Line-depth ratios

* The relations are taken from Casagrande et al. (2010).

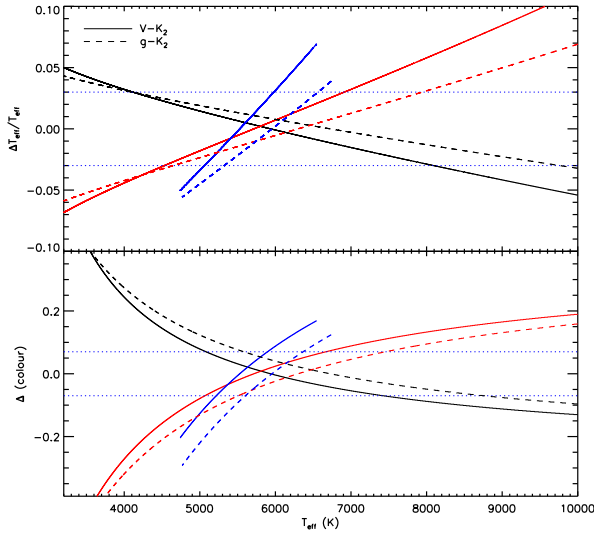


Figure 9. *Upper panel:* The relative error in T_{eff} yielded by colour ($V - K_2$) (solid lines) or ($g - K_2$) (dash lines) for a dwarf of solar metallicity if one assumes an incorrect metallicity $[\text{Fe}/\text{H}]$ of 0.5 (black), -0.8 (red), and -2.0 (blue). The blue dot lines represent a maximum acceptable relative uncertainty of 3 per cent. *Bottom panel:* Effects of metallicity on colours ($V - K_2$) and ($g - K_2$). The meaning of the different line types and colours are the same as in the upper panel. The blue dot lines represent a typical photometric error of 0.07 mag.

zero-point of IRFM effective temperature scale such that it gives consistent results with direct measurements from interferometry.

4.2 Spectroscopic effective temperatures

Santos et al. (2004) derive values of T_{eff} for 98 planet-hosting stars and 41 stars without known planets based on the excitation equilibrium of Fe I lines from high resolution spectroscopy. A total of 24 stars are found in common with our current sample of dwarfs. Their effective temperatures are on average 127 K hotter than the direct measurements, with a standard deviation s.d. = 129 K.

A uniform compilation of stellar properties for 1,040 nearby F/G/K dwarf stars derived from high resolution spectra is presented by Valenti & Fisher (2005). In their study, T_{eff} , $\log g$ and $[\text{Fe}/\text{H}]$ are estimated simultaneously by fitting the observed spectra with synthetic ones. The typical uncertainties of T_{eff} from this method is reported to be about 44 K. A comparison of common objects with the

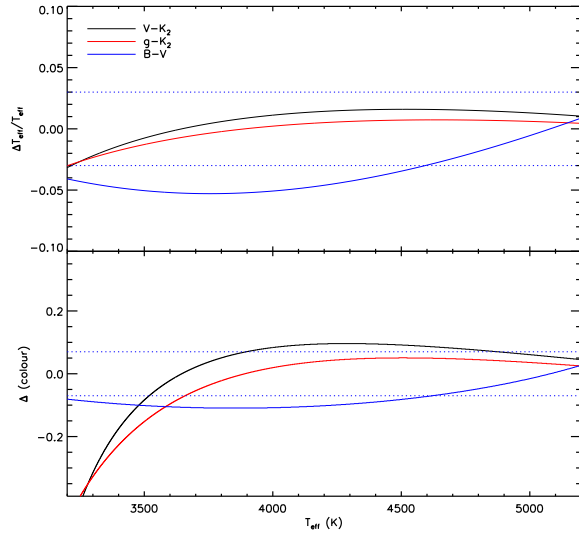


Figure 10. *Upper panel:* The relative error in T_{eff} deduced from colour ($V - K_2$) (black lines), ($g - K_2$) (red lines) and ($B - V$) (blue lines) for a dwarf of solar metallicity if the star is actually a giant, plotted as a function of T_{eff} of the dwarf. The blue dot lines represent a maximum acceptable relative uncertainty of 3.0 per cent. *Bottom panel:* The differences in colours between a giant and a dwarf for different colours as described in the upper panel, plotted as a function of T_{eff} . The blue dot lines represent a typical photometric error of 0.07 mag.

current dwarf sample yields an average difference $\Delta T_{\text{eff}} = 91$ K and a standard deviation s.d. = 129 K ($N = 59$).

On the whole, values of T_{eff} derived from high resolution spectra are on average ~ 100 K hotter than the direct measurements.

4.3 Effective temperatures deduced from line-depth ratios

To obtain effective temperatures of high precision, Kovtyukh et al. (2003, 2004, 2006, 2007) develop a method based on the observed line-depth ratios and apply the method to several hundreds dwarfs and giants stars with high resolution and high signal-to-noise ratio spectra. The temperatures derived have an internal error smaller than a few tens Kelvin. The advantage of this method is that the line-depth ratios employed are insensitive to the interstellar reddening, the spectral resolution and the rotational and micro-turbulence broadening (e.g. Kovtyukh et al. 2003). As Table 5 and Fig. 11 show, effective temperatures of dwarfs yielded by the line-

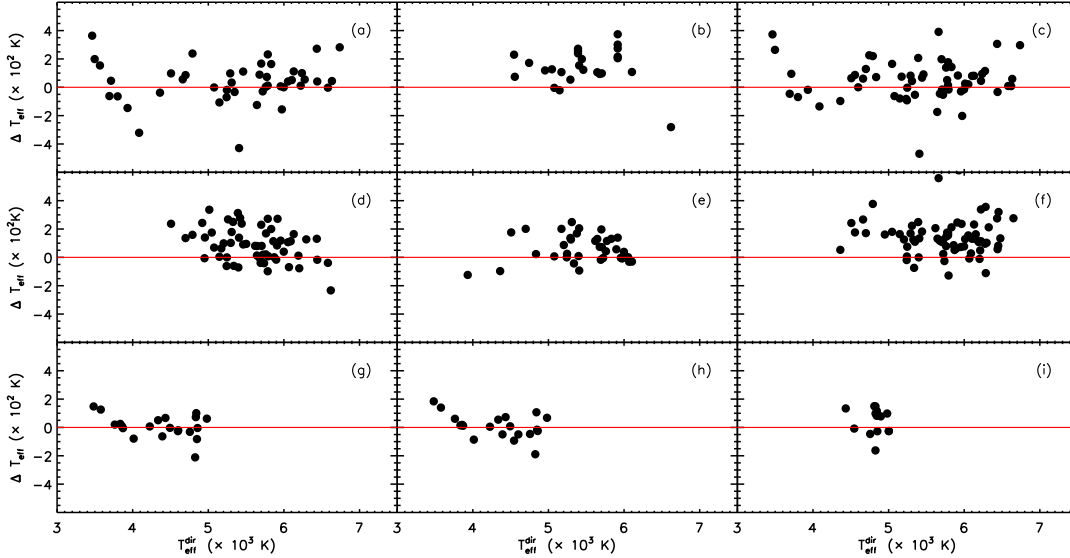


Figure 11. Differences of temperature between the alternative scales and the direct scale from interferometry are plotted against that from the direct scale, $T_{\text{eff}}^{\text{dir}}$. The top two panels are dwarfs for: (a) Alonso et al. (1996); (b) Santos et al. (2004); (c) RM05; (d) Valentin & Fischer (2005); (e) Kovtyukh et al. (2003, 2004, 2006) and (f) for Casagrande et al. (2011). The bottom panel are giants for: (g) Alonso et al. (1999); (h) RM05 and (i) Kovtyukh et al. (2006, 2007).

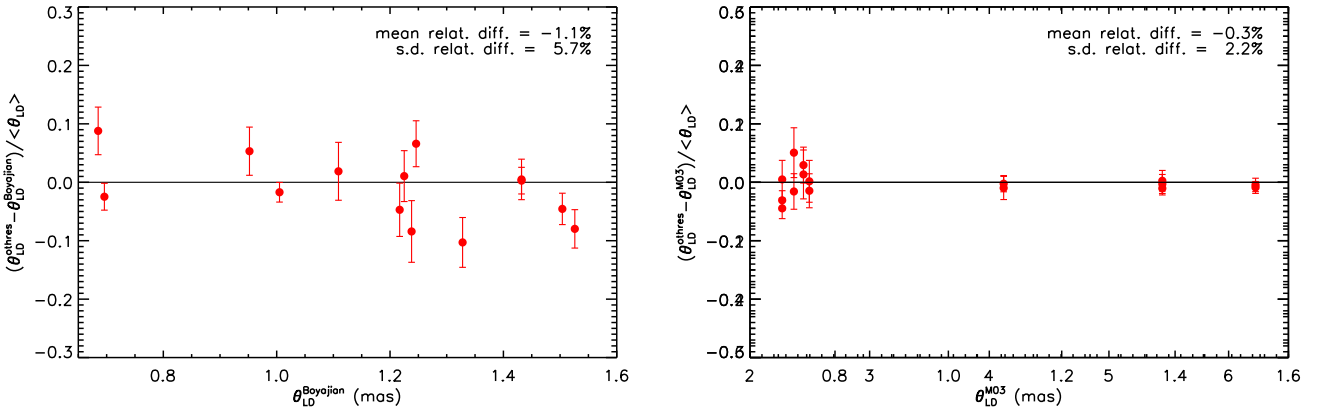


Figure 12. Relative differences of limb-darkened diameters as measured by the Boyajian's group and by others (left), and as determined by the M03 and by others (right) are plotted against the values of the Boyajian's group ($\theta_{\text{LD}}^{\text{Boyajian}}$) and those of M03 ($\theta_{\text{LD}}^{\text{M03}}$), respectively.

depth ratio technique are in general good agreement with direct measurements. The mean difference is $\Delta T_{\text{eff}} = 57$ K, with a standard deviation s.d. = 94 K ($N = 36$). For giants, effective temperatures derived by this method are slightly hotter, by an average $\Delta T_{\text{eff}} = 82$ K, along with a standard deviation s.d. = 89 K ($N = 14$). Note that the values of s.d. are quite small for both dwarfs and giants corroborating that this method based on line-depth ratios does seem to have a very high internal precision.

4.4 Remarks on the direct temperature scale

The systematic differences revealed by the above comparisons are probably caused by potential systematics in the model atmospheres or biases in the zero-point calibrations of other T_{eff} determination methods. Alternatively, they could also come from the calibrations of interferometry measurements themselves. In what follows, we discuss the potential uncertainties of direct temperature scale based

on the current compiled measurements of interferometric angular diameters.

1) Interferometric measurements: In the current work, direct measurements of T_{eff} are compiled from various studies using different telescopes. Thus the consistency between the different measurements needs to be checked. As described in Section 2, most of the angular diameter measurements for dwarfs and giants used in the current work come from the work of the Boyajian's group (B12a,b; B13) and from M03, respectively. Thus we compare respectively the angular diameters measured by Boyajian's group and by M03 with those yielded by other independent work. To do the comparisons, we present stars in our compiled catalog with multiple measurements in Table A1. As Fig. 12 shows, no systematic errors are correlated with the size of the star (i.e. θ_{LD}) in both cases. The mean and standard deviation of relative differences between the diameters measured by the Boyajian's group and by others are -1.1 and 5.7 per cent, respectively. The corresponding values of

differences between M03 and other work are -0.3 and 2.2 per cent. In both cases the means are quite small, much smaller than the standard deviations, implying that the measurements of Boyajian’s group and of M03 are consistent with the results of other independent work.

In addition, we have also checked the differences of diameters obtained with CHARA and PTI. As reported in van Belle & von Braun (2009) and B12a, diameters obtained with CHARA are $\sim (5-6) \pm 6$ per cent systematically larger than those yielded by PTI. However, we note that most of the PTI diameters included in the comparisons of the above two studies have uncertainties larger than 5 per cent. In the current work, only the diameter measurements of uncertainties less than 5 per cent are used. Here, we have done a similar comparison for stars in our sample (see Table A1) with both CHARA and PTI measurements available. We find that the CHARA diameters are on average only $\sim 1.8 \pm 6.2$ per cent larger than those yielded by PTI. Thus for sample stars adopted in the current work, the discrepancies between the CHARA and PTI diameters are much less than those reported in van Belle & von Braun (2009) and B12a, and show no significant systematics with measured diameter.

2) 1D versus 3D model atmospheres: In direct diameter measurements, corrections for limb-darkening effects are important and need to be properly applied. It is possibly true that 3D model atmospheres may present a more realistic description of the limb-darkening effects (Pereria 2013). Diameters derived using 1D model atmospheres (used for most of our sample stars) are in general $0.5 - 1.0$ per cent larger than those yielded using 3D model atmospheres (e.g. Allen Prieto et al. 2002; Bigot et al. 2006). This is confirmed by stars HD128621 and HD061421 in our sample that have diameters determined using both 1D and 3D model atmospheres (see Table A1). Thus the adoption of 1D model atmosphere measurements in the current work may induce a small systematic error compared to 3D model atmosphere measurements. However, any such systematics are likely to be quite small, on the level of $0.5 - 1.0$ per cent, far less than the measurements uncertainties (5 per cent).

3) Systematic errors related to the stellar angular diameters: For interferometric measurements, the smaller the size (angular diameter) of the star the more difficult the observations are, and thus the larger the (random plus systematic) errors of the measured diameters are. It is thus important to check whether there are any systematic errors that correlated with the size of star of concern. As reported in Casagrande et al. (2014, hereafter C14), the differences of temperatures yielded by two photometric scales, that of Casagrande et al. (2011) and Holmberg et al. (2009), and that of B12a, show a clear trend of variations (especially for stars of $\theta_{\text{LD}} \leq 1$ mas) as a function of interferometric diameter. C14 suggest that the systematic trend originates from the measurements of B12a given the nearly constant differences between temperatures from the two photometric temperature scales. To better understand the origin of this systematic trend, we have re-checked the differences between temperatures of Casagrande et al. (2011) and those from the Boyajian’s group (B12a,b, B13) using 46 common stars. As described in Section 4.1, the temperatures of Casagrande et al. (2011) are derived from the IFRM or from the T_{eff} -colour relations calibrated with the IRFM. For the very bright stars (e.g. like those in our sample), no reliable near-infrared photometric measurements are available and, as a consequence, the temperatures are derived from the T_{eff} -colour relations (mostly based on the Stömborg photometry). As the blue dots in Fig. 13 show, the differences of temperatures between those of Casagrande et al. (2011) and of B12a are

indeed essentially what C14 have seen. However, when the black dots, from B12b and B13, are also taken into consideration, the temperature differences no longer show any significant systematic trend with stellar diameter except for a nearly constant displacement (~ 130 K, see Table 5) for a wide range of stellar interferometric diameter from 0.5 to 1.5 mas. It seems that the systematic trend noted by C14 is possibly only an artifact, caused by the limited sampling and range of angular diameters of stars included in their comparison. To further check for any systematic errors that may be correlated with stellar angular size in interferometric measurements, we have carried out a similar comparison, comparing temperatures from Kovtyukh et al. (2003, 2004) with those from the Boyajian’s group (B12a,b, B13) for 24 common stars. As described in Section 4.3, temperatures from Kovtyukh et al. (2003, 2004) are obtained with line-depth ratios. Temperatures derived with this method are of a very high internal precision (to a few tens Kelvin) and are insensitive to the interstellar reddening, the spectral resolution and the rotational and micro turbulence broadening. Hence they are quite suitable to test if there are any systematic errors in the interferometric measurements that correlate with the size of the star. Again, as Fig. 13 shows, no such systematic trend is found, except for a nearly constant displacement (~ 57 K, see Table 5) for a wide diameter from 0.5 to 1.5 mas. Similarly, there are also no significant systematic errors in diameter measurements from other work for dwarfs in our sample, considering the almost zero displacement between the diameters yielded by the Boyajian’s group and by other studies, as Fig. 12 shows. For giant stars, any errors of diameter measurements caused by the differing stellar angular size are unlikely to be significant, given their large angular diameters (generally larger than 2 mas).

We conclude that: 1) The current set of diameter measurements compiled from the literature are all self-consistent; 2) The diameter measurements adopted in the current work, mostly based on 1D model atmospheres, could be possibly slightly overestimated, but only at the level of $0.5 - 1.0$ per cent; 3) The current set of measurements show no significant systematic errors that correlate with the stellar angular size.

5 COMPARISONS WITH OTHER $T_{\text{EFF}} - \text{COLOUR}$ RELATIONS

In this section, we compare the metallicity-dependent T_{eff} -colour relations presented in the current work to those from the previous studies. Fig. 16 compares the T_{eff} versus colour ($B-V$) relation for dwarfs of solar metallicity (i.e. $[\text{Fe}/\text{H}]=0$) obtained in the current calibrations with those from Casagrande et al. (2010), Boyajian et al. (2013) and MARCS model atmospheres (for $\log g = 4.0$; Gustafsson et al. 2008), as calculated by Casagrande & Vandenberg (2014). Generally, T_{eff} predicted by the relations of Casagrande et al. (2010) is ~ 100 K hotter than that of the current work, consistent with the findings in Section 4.1. The discrepancies become larger for both blue (e.g. $B - V < 0.5$ mag) and red (e.g. $B - V > 1.0$ mag) colours. The relation based on MARCS model atmospheres is in good agreement with our within a few tens of degrees Kelvin except for the blue (e.g. $B - V < 0.6$ mag, $T_{\text{eff}} > 5, 800$ K). We also compare our T_{eff} versus colour ($g - K_2$) relation for dwarfs of solar metallicity with that from MARCS model atmospheres (of $\log g = 4.0$) in Fig. 14. The results are quite similar to those in colour ($B - V$).

As described above, B13 consider the metallicity effects for colour ($B - V$) only when deriving the T_{eff} -colour relation. To

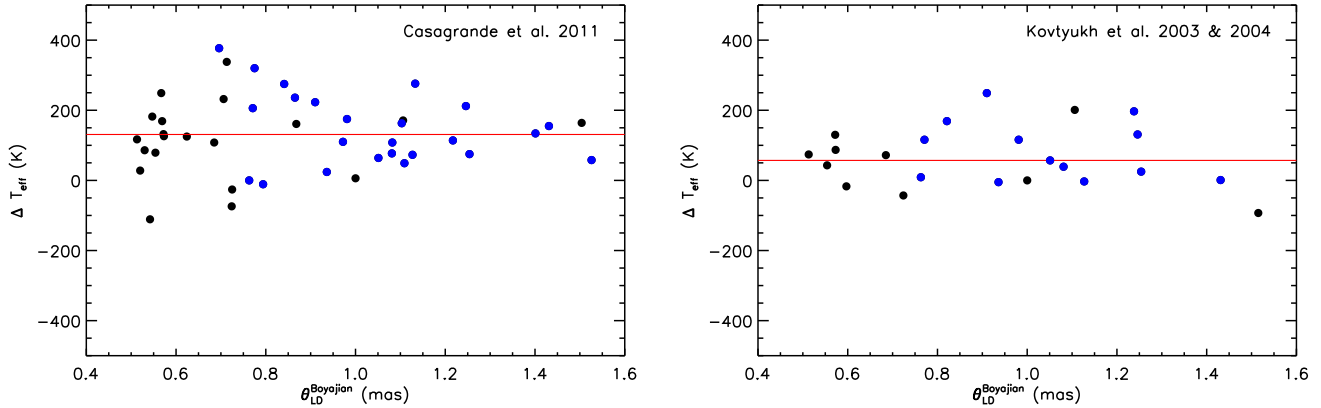


Figure 13. Differences of temperatures from Casagrande et al. (2011, left) and from Kovtyukh et al. (2003, 2004, right) with respect to the interferometric measurements of the Boyajian’s group (B12a,b, B13), plotted as a function of interferometric angular diameters measured by the Boyajian’s group. Blue dots represent interferometric measurements from B12a. Red lines delineate the mean temperature differences presented in Table 5.

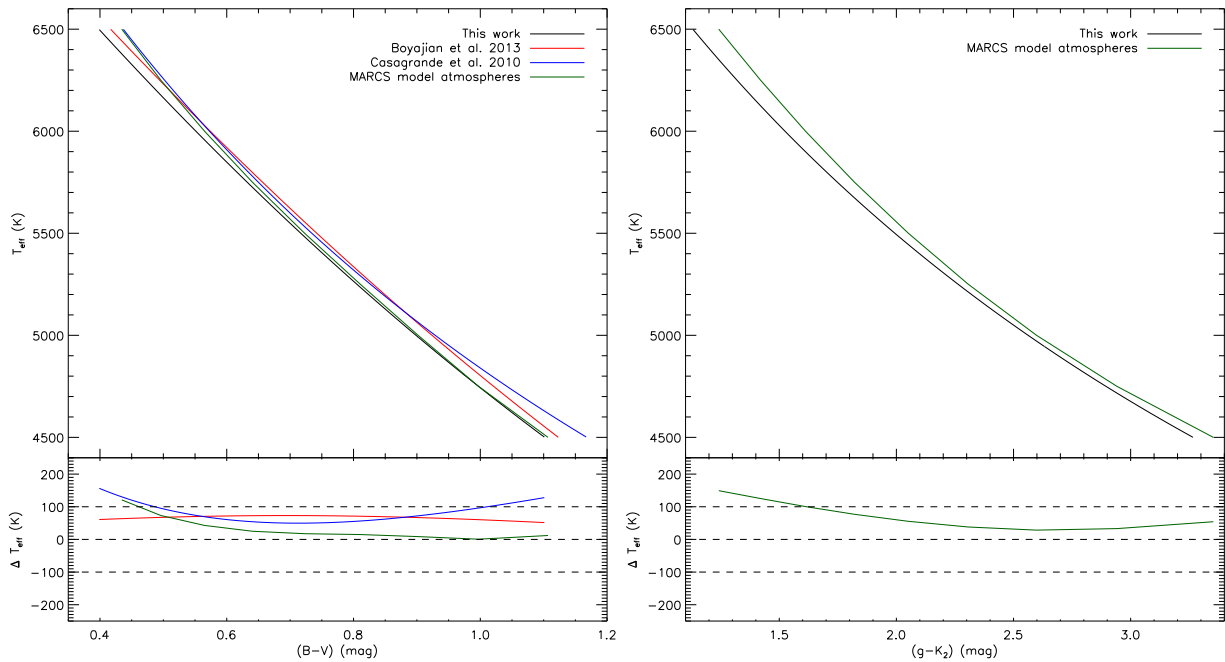


Figure 14. Comparisons of the T_{eff} –colour relations for dwarfs of solar metallicity from the current work (black) with that from B13 (red), Casagrande et al. 2010 (blue) and MARCS model atmospheres (green; assuming $\log g = 4.0$) for colour $(B - V)$ (left panel) and colour $(g - K_2)$ (right panel). The differences of predicted temperatures, ΔT_{eff} (K), as a function of colours are plotted in the lower part of each panel.

our surprise, although the samples used by B13 and the current work are quite similar (the 125 dwarfs consisting the B13 sample constitute the bulk of the current sample), temperatures predicted by the empirical relation of B13 are about 50–100 K hotter than the values calculated from the relation of the current work, for stars hotter than $T_{\text{eff}} \gtrsim 4300$ K (or $B - V \lesssim 1.20$ mag), as shown in Figs. 14 and 16 for the case of solar metallicity. We find that the residuals of the fit obtained by B13 show a systematic trend as a function of colour, as shown in Fig. 16. The systematics in the fit of B13 is fully responsible for the discrepancy between the T_{eff} – $(B - V)$ relations of B13 and of the current work.

For the giants, the T_{eff} versus colour $(V - K_2)$ relation of solar metallicity of current work is compared with that from RM05

as well as from MARCS model atmospheres (for $\log g = 2.5$), as shown in Fig. 15. Unlike the dwarfs, the relation for giants from MARCS model atmospheres is hotter than ours by ~ 100 K. The relation of RM05 is in excellent agreement with ours in their applicable range $(V - K_2 < 3.29$ mag).

6 APPLICATIONS

6.1 Colours of the Sun

It is not an easy task to measure colours of the Sun, being such a bright and extended source. Most measurements of the solar

Table 6. Colours of the Sun

Colour	This Work	CBC96 ^{*a}	AAM96 [*]	SF00 [*]	RM05 [*]	HFP06 [*]	C10 [*]	R12 [*]	CV15 ^{*b}
$U - V$	0.791 ± 0.070	0.770	0.770 ± 0.036	–	–	0.815 ± 0.066	–	0.819 ± 0.023	0.770
$B - V$	0.623 ± 0.037	0.630	0.615 ± 0.020	0.626 ± 0.018	0.619	0.642 ± 0.016	0.641 ± 0.024	0.653 ± 0.005	0.621
$V - R_J$	0.526 ± 0.036	–	0.525 ± 0.020	–	–	–	–	–	–
$R_J - I_J$	0.323 ± 0.026	–	0.325 ± 0.020	–	–	–	–	–	–
$V - I_J$	0.849 ± 0.055	–	0.850 ± 0.020	–	–	–	–	–	–
$V - R_C$	0.348 ± 0.025	–	–	–	0.351	0.354 ± 0.010	0.359 ± 0.010	0.356 ± 0.003	0.361
$V - I_C$	0.665 ± 0.045	–	–	–	0.682	0.688 ± 0.014	0.690 ± 0.016	0.701 ± 0.003	0.688
$R_C - I_C$	0.318 ± 0.024	–	–	–	0.330	0.332 ± 0.08	0.333 ± 0.010	–	0.327
$V - J$	1.068 ± 0.060	–	–	–	–	–	–	–	–
$V - H$	1.362 ± 0.083	–	–	–	–	–	–	–	–
$V - K$	1.437 ± 0.080	–	–	–	–	–	–	–	–
$V - J_2$	1.125 ± 0.060	–	–	–	1.141	1.151 ± 0.035	1.180 ± 0.021	–	1.164
$V - H_2$	1.366 ± 0.081	–	–	–	1.396	1.409 ± 0.035	1.460 ± 0.023	–	1.452
$V - K_2$	1.472 ± 0.080	–	–	–	1.495	1.505 ± 0.041	1.544 ± 0.018	–	1.537
$g - r$	0.419 ± 0.036	–	–	–	–	0.450 ± 0.020	–	–	0.426
$g - J$	1.313 ± 0.075	–	–	–	–	–	–	–	–
$g - H$	1.611 ± 0.102	–	–	–	–	–	–	–	–
$g - K$	1.689 ± 0.095	–	–	–	–	–	–	–	–
$g - J_2$	1.370 ± 0.075	–	–	–	–	–	–	–	1.425
$g - H_2$	1.618 ± 0.093	–	–	–	–	–	–	–	1.713
$g - K_2$	1.723 ± 0.096	–	–	–	–	–	–	–	1.798

* References: CBC96 – Colina, Bohlin & Castelli (1996); AAM96 – Alonso, Arribas & Martínez-Roger (1996); SF00 – Sekiguchi & Fukugita (2000); HFP06 – Holmberg, Flynn & Portinari (2006); C10 – Casagrande et al. (2010) and R12 – Ramírez et al. (2012); CV15 – Casagrande & Vandenberg (2014).

^a Those colours of the Sun are obtained from the real solar spectrum directly.

^b Those colours of the Sun are obtained using the MARCS synthetic solar spectrum (for microturbulence velocity $\xi = 1 \text{ km s}^{-1}$, $T_{\text{eff}} = 5777 \text{ K}$, $\log g = 4.44$ and $[\text{Fe}/\text{H}] = 0$).

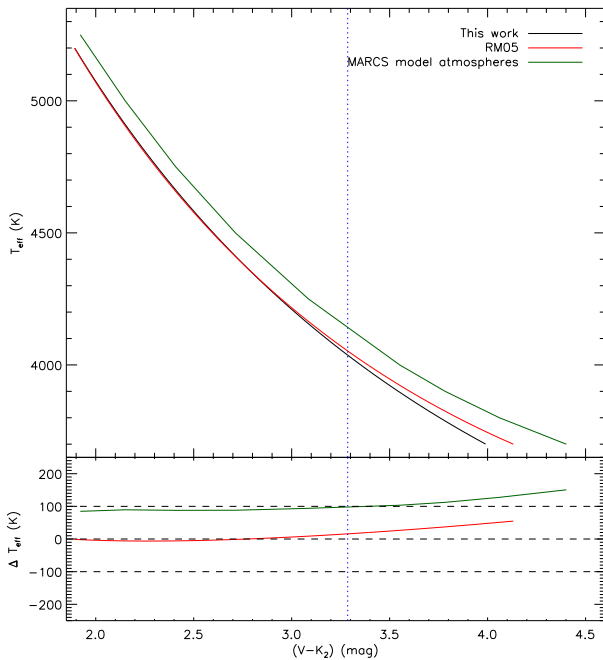


Figure 15. Comparisons of the $T_{\text{eff}}-(V - K_2)$ relation for giants of solar metallicity presented in the current work (black) with that from RM05 (red) and MARCS model atmospheres (green; $\log g = 2.5$). The lower part of the panel shows the differences of T_{eff} , ΔT_{eff} (K), between the values predicted by relations from other studies and by ours as a function of colour. The dashed blue line indicates the upper applicable range of colour range of the relation of RM05 $V - K_2 = 3.29$.

colours are made indirectly, either using the *solar twins* or the interpolating empirical relations (e.g. the T_{eff} -colour-metallicity relations) to the solar values based on samples of stars with well determined physical properties (e.g. Alonso et al. 1996; Sekiguchi & Fukugita 2000; RM05; Holmberg et al. 2006; Casagrande et al. 2010; Ramírez et al. 2012). However, essentially all the effective temperature scales of the aforementioned work are based on temperatures deduced by indirect methods (e.g. the IRFM or spectroscopy). Consequently, there could be a systematic errors in the estimated colours of the Sun. Using the empirical calibration based on direct effective temperature measurements from interferometry presented in the current work, we have derived the colours of the Sun assuming a solar effective temperature $T_{\text{eff}} = 5,777 \text{ K}$ and metallicity $[\text{Fe}/\text{H}] = 0^{10}$. The results are presented in Table 6 and compared to literature values.

Table 6 shows that, as expected, our newly deduced colours of the Sun are systematic bluer than the recent determinations of Casagrande et al. (2010), deduced with the same method but based on an IRFM effective temperature scale, which is about 130 K higher than the direct scale derived here, as shown in Fig. 11 (f) and Table 5. As shown in Table 6, our newly deduced colour ($B - V$) of the Sun agrees well with the direct measurement of Colina, Bohlin & Castelli (1996). Using a similar approach as ours, Sekiguchi & Fukugita (2000) also find similar result. We warn that the colours of the Sun presented in the current work that involves bands transformed from measurements in other bands, e.g. those involving the SDSS gr or the 2MASS $J_2H_2K_2$ bands, may suffer from large errors (both random and systematic), considering the possible errors propagated by those transformations. Of course, as discussed

¹⁰ Here we use the empirical relations deduced excluding the early-type stars.

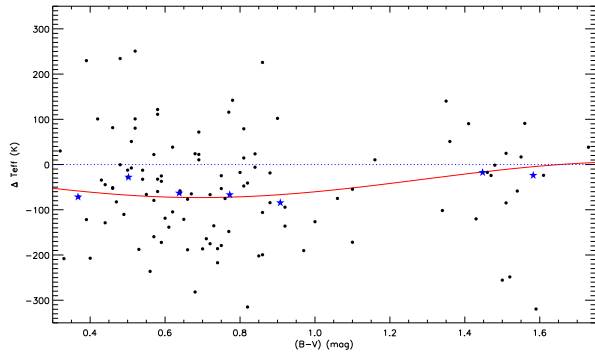


Figure 16. Differences of effective temperatures deduced from the $T_{\text{eff}}-(B-V)$ relation of the current work and those from the relation of B13 for the solar metallicity, plotted against $(B-V)$ (red line). Black dots represent the residuals ($T_{\text{eff}} - T_{\text{eff}}^{\text{fit}}$) of fit in the calibration of B13 and blue stars are the median residuals in the individual colour bins.

above, the interferometry measurements themselves are not entirely free of potential systematics. This should be kept in mind when using the colours of the Sun presented in the current work.

6.2 Calibration of temperature scales for stellar spectroscopic surveys

In large scale medium- to low-resolution stellar spectroscopic surveys, such as the SDSS/SEGUE and LSS-GAC, effective temperature T_{eff} is generally estimated simultaneously with other stellar atmospheric parameters including metallicity $[\text{Fe}/\text{H}]$ and surface gravity $\log g$, by, for example, template matching with either empirical or synthetic spectra (e.g. Lee et al. 2008; Luo et al. 2015; Xiang et al. 2014). As shown in Section 4, effective temperatures thus determined could deviate from the true values by hundreds Kelvin. In this subsection, we attempt to calibrate the temperature scales of two recent spectroscopic surveys: the SDSS and LSS-GAC, using the empirical T_{eff} -colour relations presented in the current work and examine if there are any systematic errors in the effective temperatures yielded by those surveys. The results are presented in Table 7, including the average difference ΔT_{eff} between the values of T_{eff} as yielded by the pipelines of those surveys and the values deduced from the empirical relations presented in the current work, along with the standard deviation of the difference, s.d., the median spectral signal-to-noise ratios (SNRs) of the stars used in the comparison, the number of stars N used, and the method used by the pipeline to estimate effective temperatures.

- **SDSS:** The SDSS/SEGUE Stellar Parameters Pipeline (SSPP; Lee et al. 2008a, 2008b; Allende Prieto et al. 2008; Smolinski et al. 2011) estimates effective temperatures utilizing multiple approaches. Each method has its favoured applicable range in colour ($g-r$) and SNR. The final adopted T_{eff} is the average of results from all methods. In order to calibrate the SSPP effective temperatures, we select stars of spectral SNRs > 30 and reddening $E(B-V) < 0.05$ mag, as given by the extinction map of SFD98, to minimize the effects of uncertainties of reddening corrections, from the ninth data release of SDSS (hereafter DR9; Ahn et al. 2012). Following the results presented in Section 3, we use the $T_{\text{eff}}-(g-K_2)$ relation to derive photometric temperatures of those selected SDSS stars (with metallicities yielded by the SSPP). To obtain the K_2 magnitudes and reliable intrinsic colours of those stars, they are cross-matched with the 2MASS photometric cata-

log. For stars with a match, only those with a 2MASS flag *ph_qual* flagged by ‘A’ in K_s -band and with a K_s -band photometric error less than 0.05 mag, and at the same time with a SDSS g -band magnitude greater than 14.0 mag (to avoid potential saturation), and a g -band photometric error smaller than 0.02 mag, are retained. Finally we select 10,682 dwarf stars with $\log g \geq 3.5$ and 280 giant stars with $\log g < 3.5$. The photometric temperatures of those stars are then calculated using the $T_{\text{eff}}-(g-K_2)$ relation presented in Section 3, subject to the applicability ranges in colour and metallicity as shown in Tables 3 and 4. A comparison of the T_{eff} between the SDSS DR9 adopted values and the photometric values yielded by our direct empirical calibration is presented in Fig. 17. On average, the DR9 adopted effective temperatures are systematically hotter than our values by 147 and 158 K for dwarfs and giants, respectively (cf. Table 7). The systematic offset of ~ 150 K found here is easily understood considering the fact that the SSPP re-scales temperatures yielded by each method to match with the IRFM scale of Casagrande et al. (2010), which has been shown to be too hot by 131 K compared to the direct effective temperature scale (cf. Section 4, Fig. 11 (f) and Table 5). The standard deviations of the differences are smaller than 80 K, for both dwarfs and giants, suggesting that the uncertainties of ~ 50 K reported by Ahn et al. (2012) for stars of spectral SNRs > 30 are reasonable estimated. Finally, we caution that the systematic offset, ΔT_{eff} , is not a constant but has some weak dependence on temperature.

- **LSS-GAC:** As a major component of the on-going LAMOST Galactic surveys, the LSS-GAC (Liu et al. 2014) aims to collect optical ($\lambda\lambda 3700-9000$), low resolution ($R \sim 1,800$) spectra for a statistically complete sample of over a million stars of all colours in the magnitude range $14.0 \leq r < 17.8$ mag (18.5 mag for limited fields), distributed in a continuous sky area of $\sim 3,400$ sq.deg, covering Galactic longitudes $150 < l < 210^\circ$ and latitudes $|b| < 30^\circ$ under good observing conditions (dark or grey lunar nights). In addition, with a similar target selection algorithm, over 1.5 million very bright stars brighter than 14.0 mag (and normally fainter than 9.0 mag), will be observed utilizing bright lunar nights. At present, two stellar parameter pipelines, the LAMOST Stellar Parameter Pipeline (LASP; Wu et al. 2014; Luo et al. 2015) and the LAMOST Stellar Parameter at Peking University (LSP3; Xiang et al. 2014), have been developed that deliver spectral classifications and deduce stellar radial velocities and atmospheric parameters from collected spectra. Both pipelines apply a template matching technique to estimate the atmospheric parameters, except that the LASP uses the ELODIE library (Prugniel & Soubiran 2001; Prugniel et al. 2007) spectra of very high resolution ($R \sim 4,200$), obtained with an echelle spectrograph, after degrading the spectral resolution to match that of LAMOST spectra, while the LSP3 adopts the MILES spectral library (Sánchez-Blázquez et al. 2006) consisting of accurately flux-calibrated spectra of spectral resolution comparable to that of LAMOST spectra. Both libraries contain a similar number of stars ($\sim 1,000$) that cover similar ranges in stellar atmospheric parameters. The Pilot and Regular Surveys of LSS-GAC were initiated in September 2011 and 2012, respectively. By the summer of 2013, over one million spectra of good quality, SNR (7450\AA) ≥ 10 , have been collected (Yuan et al. 2014). The Regular Survey is expected to last for 5 years.

As in the case above for the SDSS DR9 data, we select the stars from the LSS-GAC Value-added Data Release 1 (DR1; Yuan et al. 2014) of good LAMOST spectral SNRs (4650\AA) > 15 and low extinction [$E(B-V) < 0.05$ mag] that also have high precision photometry in K_s band from the 2MASS and g -band from the XSTPS-GAC (Zhang et al. 2013, 2014; Liu et al. 2014). Fi-

Table 7. Comparisons with the effective temperature yielded by the pipelines of SDSS/SEGUE and LSS-GAC

Source	ΔT_{eff} (K)	s.d. (K)	$\langle \text{SNR} \rangle$	N	Method
Dwarf stars					
SDSS DR9 (Ahn et al. 2012)	147	75	58	10682	Multiple methods ^a
LSP3 (Xiang et al. 2014)	12	120	37	26953	Template matching ^b
LASP (Wu et al. 2014)	-6	100	37	26562	Template matching ^c
Giant stars					
SDSS DR9 (Ahn et al. 2012)	156	84	57	280	Multiple methods ^a
LSP3 (Xiang et al. 2014)	44	95	36	3747	Template matching ^b
LASP (Wu et al. 2014)	-15	76	36	3413	Template matching ^c

^a Effective temperatures yielded by individual methods are scaled to match those given by the IRFM effective temperature scale of Casagrande et al. (2010).

^b Using the MILES spectral library as templates.

^c Using the ELODIE spectral library as templates.

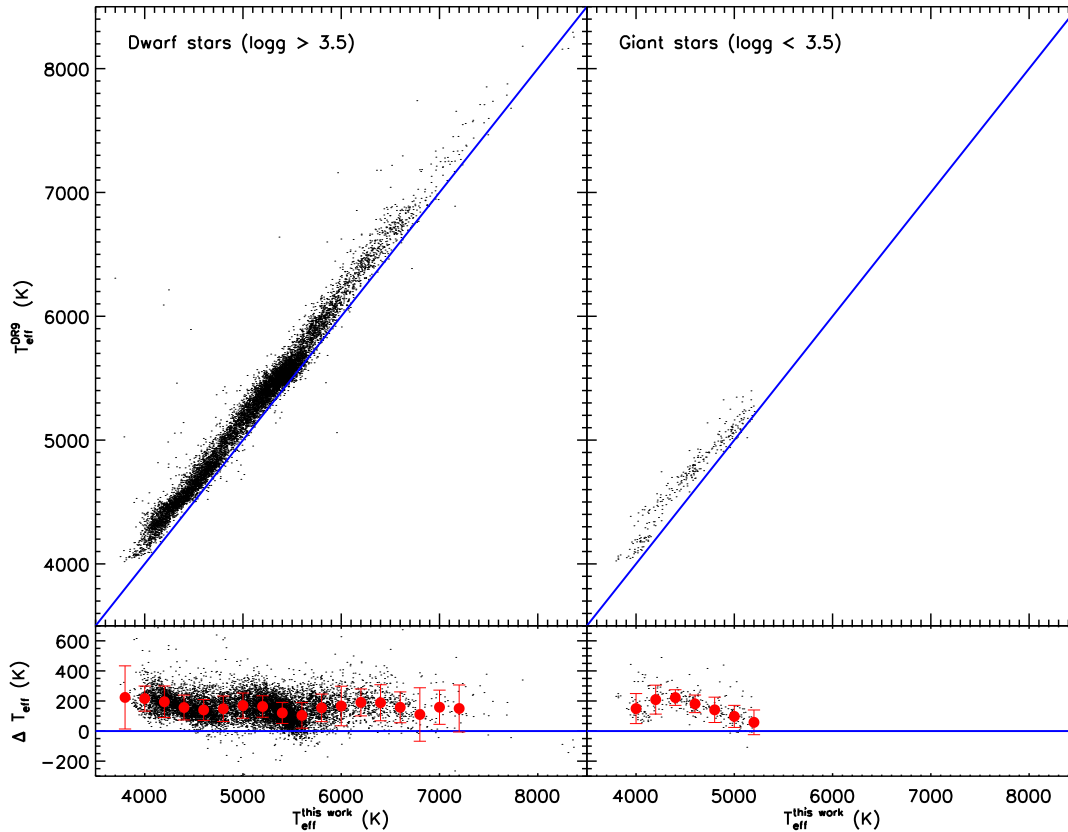


Figure 17. Comparison of effective temperatures adopted by the SDSS DR9 and those derive from our $T_{\text{eff}}-(g - K_2)$ relation. The differences, $\Delta T_{\text{eff}} = (T_{\text{eff}}^{\text{DR9}} - T_{\text{eff}}^{\text{this work}})$, are plotted at the bottom (with red dots and error bars representing the means and standard deviations of differences in the individual temperature bins). The left panel is for dwarfs of $\log g > 3.5$ and the right for giants of with $\log g < 3.5$.

nally, we derive values of T_{eff} based on our empirical relation in colour ($g - K_2$) for $\sim 26,000$ dwarfs and 3,000 giants selected from the LSS-GAC DR1 (using metallicities yielded by LSP3). Effective temperatures yielded by the LSP3 and LASP are compared respectively in Figs. 18 and 19 to those derived from our empirical relation. On the whole, for both dwarfs and giants, values of T_{eff} yielded by the LSP3 and LASP are consistent within a few tens Kelvin with the results given by our empirical calibration (cf. Table 7). However, the agreement is less satisfactory for very hot or cool stars. For the LSP3, it overestimates the effective temperature about by 100 – 200 K for stars hotter than 6500 K or those cooler

than 4000 K, dwarfs or giants likewise. In Xiang et al. (2014), they correct those systematics in their final released results using the empirical calibration presented here. For the LASP, the deviations for hot stars are insignificant, but systematics on the level of ~ 100 –200 K are detected for stars cooler than 4500 K, for both dwarfs and giants but with opposite trends. For dwarfs, the LASP underestimates their effective temperatures, while for giants it does the opposite. Most of the systematics seen in LSP3 or LASP parameters are propagated from the uncertainties of effective temperature scales of template libraries employed by those pipelines (MILES or ELODIE). Ideally, in future, one can correct the systematics in ef-

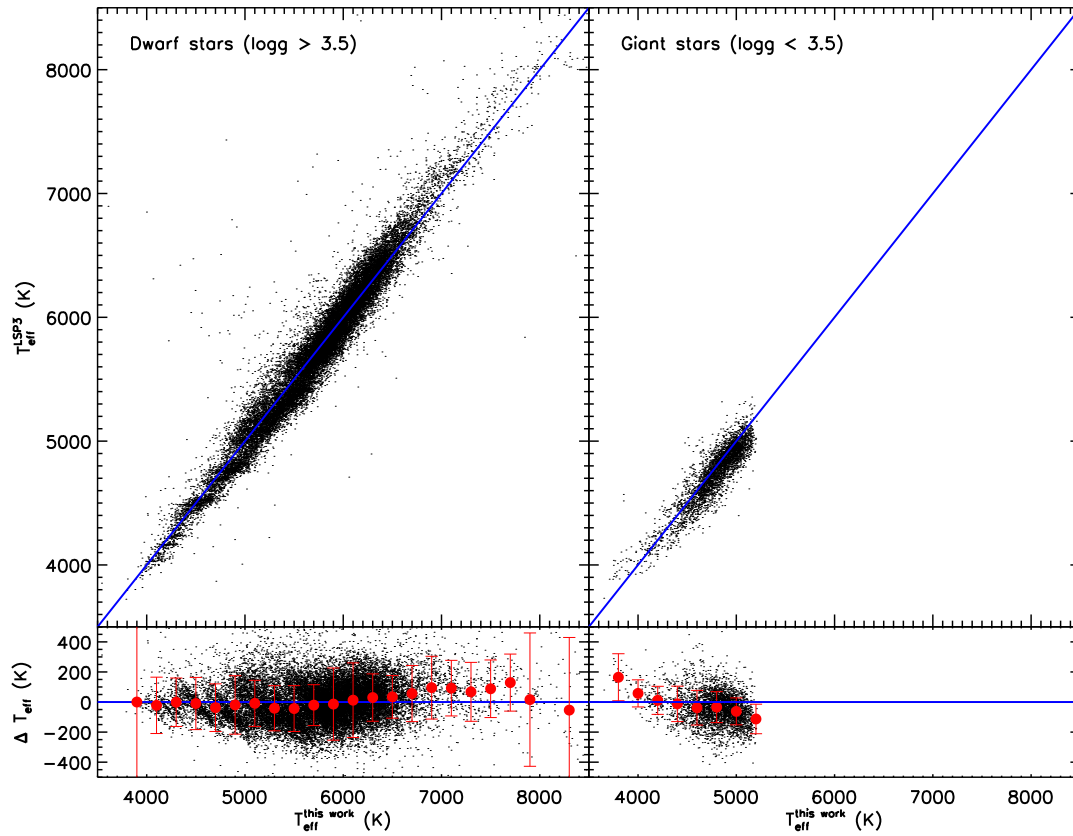


Figure 18. Similar to Fig. 15 but for the LSP3.

fective temperature scale of those template libraries directly using the empirical calibration presented here.

To conclude, the empirical metallicity-dependent T_{eff} -colour relations presented in the current work can be used to provide accurate, unbiased estimates of T_{eff} for millions of stars targeted by modern large stellar spectroscopic surveys with high efficiency, especially relation in the colour ($g - K_2$), given its weak dependence on both metallicity and luminosity. To apply those photometric calibrations, accurate estimates of the interstellar extinction are essential especially for disk stars. Fortunately, with the multi-band photometric data now available, one can obtain highly accurate estimates of extinction towards individual stars using a variety of techniques, such as the spectral energy (SED) fitting method (e.g. Chen et al. 2014) or the ‘star-pair’ technique (e.g. Yuan et al. 2013). For example, using the SED fitting technique, Chen et al. (2014) estimate extinction values towards more than 13 million stars, covering the entire footprint of the XSTPS-GAC area (over 6000 sq. deg.), based on the multi-band photometries from the XSTPS-GAC in the optical, and the 2MASS and WISE (Wright et al. 2010) in the infrared.

7 CONCLUSIONS

Based on nearly two hundred dwarf (luminosity classes: IV/V) and giant (luminosity classes: II/III) stars with direct effective temperature measurements of better than 2.5 per cent collected from the literature, we have derived metallicity-dependent T_{eff} -colour rela-

tions in twenty-one colours for dwarfs and eighteen colours for giants in four photometric systems (the Johnson, Cousins, SDSS and 2MASS). The calibrations have typical percentage residuals of 2.0 and 1.5 per cents for dwarf and giant stars, respectively. Restricted by the available calibration sample stars, at present, the calibrations are limited to the metal-rich stellar populations, although a couple of dwarfs of metallicities $[\text{Fe}/\text{H}] \sim -2.0$ included by our sample providing some constraints on the relations at such low metallicities. We expect more metal-poor stars (both dwarfs and giants) will be observed with the LBOI in the future and thus improve the calibrations at low metallicities.

The effects of metallicity on T_{eff} can be well understood, which has well explained by R05 using synthetic spectra. We explore quantitatively the effects of metallicity and luminosity on effective temperatures derived from colour ($g - K_2$) or ($V - K_2$). Generally, for disk stars ($[\text{Fe}/\text{H}] > -1.0$), both colours show only weak dependence on both metallicity and luminosity. However, for halo stars ($[\text{Fe}/\text{H}] \sim -2.0$), the metallicity effects are significant.

A detailed comparison between the empirical, direct temperature scale presented in the current work with those in the literature is presented. We find that the IRFM effective temperature scales of Alonso et al. (1996, 1999) and RM05 match the current one within few tens Kelvin, while that of Casagrande et al. (2010, 2011) is about 130 K hotter. This discrepancies amongst different IRFM scales are likely caused by the different zero-points adopted. We also find that spectroscopic effective temperature scales (such as those based on the ‘excitation balance of iron lines’, spectral template matching or line-depth ratios) are 50–130 K hotter than the di-

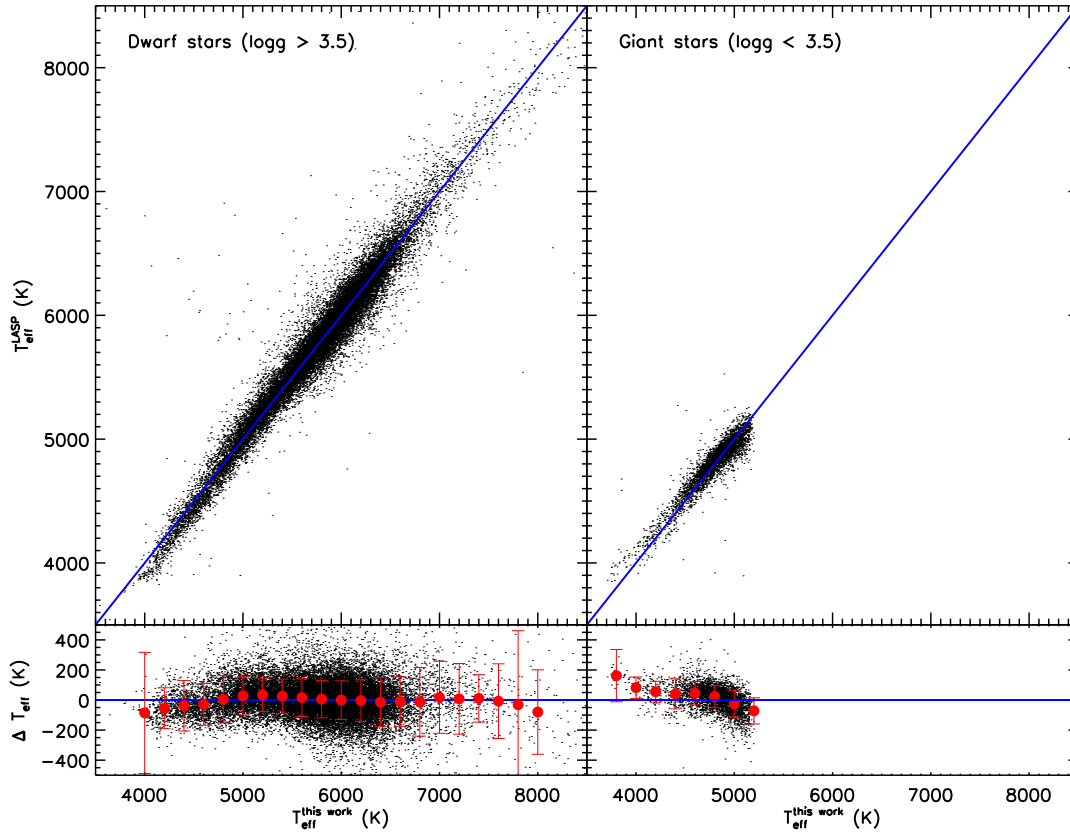


Figure 19. Similar to Fig. 15 but for the LASP.

rect effective temperature scale. The differences between the direct effective temperature scale and other indirect effective temperature scales could be due to systematics in model atmospheres or zero-point calibrations of those indirect scales, although potential biases in the calibrations of interferometry measurements themselves cannot be ruled out entirely. In addition, we find that the metallicity-dependent $T_{\text{eff}}-(B - V)$ relation derived by B13 is inconsistent with the direct effective temperature scale presented here. We find that this is likely caused by the systematics in the fit of B13.

As an example, we present twenty-one colours of the Sun, deduced from the current calibrations assuming a solar $T_{\text{eff}} = 5777$ K and $[\text{Fe}/\text{H}] = 0$. Also using the calibration in colour ($g - K_2$), we investigate possible systematics in effective temperatures yielded by two of the currently on-going large scale stellar spectroscopic surveys: the SDSS and LSS-GAC. The effective temperatures delivered by the SSPP pipeline of SDSS seems to have systematically overestimated the effective temperatures by approximately 150 K. The cause of this discrepancy can be attributed to the fact that the SSPP calibrate all effective temperature determinations to match the IRFM scale of Casagrande (2010). For the LSS-GAC, effective temperatures given by both the LSP3 and LASP agree well with the photometric values yielded by our empirical calibration, although some deviations are seen in the results of very hot or cool stars.

With high precision photometry now available from the SDSS, XSTPS-GAC, PanSTARRS in optical and from 2MASS in the infrared, we expect that the $T_{\text{eff}}-(g - K_2)$ calibration presented in the current work can be an invaluable tool for the determinations

of effective temperature for large numbers of stars targeted by the currently on-going or upcoming large scale stellar spectroscopic surveys.

ACKNOWLEDGEMENTS

We thank the referee, Dr. M. Bessell, for constructive suggestions that improve the manuscript significantly. This work is supported by National Key Basic Research Program of China 2014CB845700.

The Guoshoujing Telescope (the Large Sky Area Multi-Object Fiber Spectroscopic Telescope, LAMOST) is a National Major Scientific Project built by the Chinese Academy of Sciences. Funding for the project has been provided by the National Development and Reform Commission. LAMOST is operated and managed by the National Astronomical Observatories, Chinese Academy of Sciences.

This work has made use of data products from the Sloan Digital Sky Survey (SDSS), Two Micron All Sky Survey (2MASS), Wide-field Infrared Survey Explorer (WISE) and SIMBAD database, operated at CDS, Strasbourg, France.

REFERENCES

Ahn, C.P., et al. 2012, ApJS, 203, 21
 Allende Prieto, C., Asplund, M., García López, R.J., & Lambert, D.L. 2002, ApJ, 567, 544

- Allende Prieto, et al. 2008, *AJ*, 136, 2070
- Alonso, A., Arribas, S., & Martínez-Roger, C. 1996, *A&A*, 313, 873
- Alonso, A., Arribas, S., & Martínez-Roger, C. 1999, *A&AS*, 140, 261
- Baines, E.K., McAlister, H.A., ten Brummelaar, T.A., Turner, N.H., Sturmman, J., Sturmman, L., Ridgway, S.T. 2008, *ApJ*, 682, 577
- Baines, E.K., McAlister, H.A., ten Brummelaar, T.A., Sturmman, J., Sturmman, L., Turner, N.H., Ridgway, S.T. 2009, *ApJ*, 701, 154
- Baines, E.K., Armstrong, J.T., & Schmitt, H.R. 2010, *SPIE*, 7734, 3 (Ba10a)
- Baines, E.K., 2010, *ApJ*, 710, 1365 (Ba10b)
- Baines, E.K., et al. 2011, *ApJ*, 743, 130
- Bessell, M.S., & Brett, J.M. 1988, *PASP*, 100, 1134
- Bessell, M.S., Castelli, F., & Plez, B. 1998, *A&A*, 333, 231
- Bigot, L., Kervella, P., Thévenin, F., & Ségransan, D. 2006, *A&A*, 446, 635
- Blackwell, D.E., & Shallis, M.J. 1977, *MNRAS*, 180, 177
- Blackwell, D.E., Petford, A.D., Arribas, S., Haddock, D.J., & Selby, M.J. 1990, *A&A*, 232, 396
- Bohlin, R.C. 2010, *AJ*, 139, 1515
- Boyajian, T. S., et al. 2009, *ApJ*, 691, 1243
- Boyajian, T.S., et al. 2012, *ApJ*, 746, 101 (B12a)
- Boyajian, T.S., et al. 2012, *ApJ*, 757, 112 (B12b)
- Boyajian, T.S., et al. 2013, *ApJ*, 771, 40 (B13)
- Carpenter, J.M. 2001, *AJ*, 121, 2851
- Casagrande, L., Portinari, L., & Flynn, C. 2006, *MNRAS*, 373, 13
- Casagrande, L., Ramírez, I., Meléndez, J., Bessell, M., & Asplund, M. 2010, *A&A*, 512, A54
- Casagrande, L., Schönrich, R., Asplund, M., Cassisi, S., Ramírez, I., Meléndez, J., Bensby, T., Feltzing, S. 2011, *A&A*, 530, A138
- Casagrande, L., & VandenBerg, D.A. 2014, *MNRAS*, 444, 392
- Casagrande, L., et al. 2014, *MNRAS*, 439, 2060
- Castelli, F. 1999, *A&A*, 346, 564
- Chen, B.-Q. et al. 2014, arXiv:1406.3996
- Code, A.D., Bless, R.C., Davis, J., & Brown, R.H. 1976, *ApJ*, 203, 417
- Colina, L., Bohlin, R.C., & Castelli, F. 1996, *AJ*, 112, 307
- Creevey, O.L., et al. 2012, *A&A*, 537, A111
- Cusano, F., et al. 2012, *A&A*, 539, A58
- Demarque, P.R., & Larson, R.B. 1964, *ApJ*, 140, 544
- Dotter, A., Chaboyer, B., Jevremović, D., Kostov, V., Baron, E., Ferguson, J.W. 2008, *ApJS*, 178, 89
- Ducati, J. R. 2002, *VizieR Online Data Catalog*, 2237, 0
- Eisenstein, D.J., et al. 2011, *AJ*, 142, 72
- Fitzpatrick, E.L. 1999, *PASP*, 111, 63
- Girardi, L., Bertelli, G., Bressan, A., Chiosi, C., Groenewegen, M.A.T., Marigo, P., Salasnich, B., Weiss, A. 2002, *A&A*, 391, 195
- Girardi, L., Grebel, E.K., Odenkirchen, M., & Chiosi, C. 2004, *A&A*, 422, 205
- González Hernández, J.I., & Bonifacio, P. 2009, *A&A*, 497, 497
- Gratton, R. G., Carretta, E., & Castelli, F. 1996, *A&A*, 314, 191
- Gray, D. F. 1992, *The Observation and Analysis of Stellar Photospheres* (Cambridge: Cambridge Univ. Press)
- Gustafsson, B., Edvardsson, B., Eriksson, K., Jørgensen, U.G., Nordlund, Å, Plez, B., 2008, *A&A*, 486, 951
- Heiter, U., 2002, *A&A*, 392, 619
- Holmberg, J., Flynn, C., & Portinari, L. 2006, *MNRAS*, 367, 449
- Holmberg, J., Nordström, B., & Andersen, J. 2009, *A&A*, 501, 941
- Houdashelt, M. L., Bell, R. A., & Sweigart, A. V. 2000, *AJ*, 119, 1448
- Huber, D., et al. 2012, *ApJ*, 760, 32
- Jester, S., et al. 2005, *AJ*, 130, 873
- Kaiser, N., et al. 2002, *SPIE*, 4836, 154
- Keller, S.C., et al. 2007, *PASA*, 24, 1
- Koleva, M., & Vazdekis, A. 2012, *A&A*, 538, A143
- Kovtyukh, V.V., Soubiran, C., Belik, S.I., & Gorlova, N.I. 2003, *A&A*, 411, 559
- Kovtyukh, V.V., Soubiran, C., & Belik, S.I. 2004, *A&A*, 427, 933
- Kovtyukh, V.V., Soubiran, C., Bienaymé, O., Mishenina, T.V., & Belik, S. I. 2006, *MNRAS*, 371, 879
- Kovtyukh, V.V. 2007, *MNRAS*, 378, 617
- Kučinskas, A., Hauschildt, P.H., Ludwig, H.G., Brott, I., Vansevičius, V., Lindegren, L., Tanabé, T., Allard, F., 2005, *A&A*, 442, 281
- Lee, Y.-S., et al. 2008, *AJ*, 136, 2022 (2008a)
- Lee, Y.S., et al. 2008, *AJ*, 136, 2050 (2008b)
- Liu X. -W., et al., 2014, in Feltzing S., Zhao G., Walton N., White-lock P., eds, *Proc. IAU Symp. 298, Setting the scene for Gaia and LAMOST*, Cambridge University Press, pp. 310-321, preprint (arXiv: 1306.5376)
- LSST Science Collaboration. 2009, arXiv:0912.0201
- Luo, et al. 2015, *RAA*, 15, 1095
- Maestro, V., et al. 2013, *MNRAS*, 434, 1321
- Martins, L.P., & Coelho, P. 2007, *MNRAS*, 381, 1329
- Massa, D., Savage, B.D., & Fitzpatrick, E.L. 1983, *ApJ*, 266, 662
- Mermilliod, J.-C., Mermilliod, M., & Hauck, B. 1997, *A&AS*, 124, 349
- Monnier, J.D., et al. 2007, *Science*, 317, 342
- Mozurkewich, D., et al. 2003, *AJ*, 126, 2502 (M03)
- Norris, J.E., et al. 2013, *ApJ*, 762, 25
- North, P., Berthet, S., & Lanz, T. 1994, *A&A*, 281, 775
- North, J.R., et al. 2007, *MNRAS*, 380, L80
- Pereira, T.M.D., Asplund, M., Collet, R., Thaler, I., Trampedach, R., Leenaarts, J., 2013, *A&A*, 554, AA118
- Perryman, M.A.C., et al. 2001, *A&A*, 369, 339
- Prugniel, P., & Soubiran, C. 2001, *A&A*, 369, 1048
- Prugniel, P., Soubiran, C., Koleva, M., & Le Borgne, D. 2007, arXiv:astro-ph/0703658
- Ramírez, I., & Meléndez, J. 2005, *ApJ*, 626, 465 (RM05)
- Ramírez, et al. 2012, *ApJ*, 752, 5
- Ruchti, G.R., Bergemann, M., Serenelli, A., Casagrande, L., & Lind, K. 2013, *MNRAS*, 429, 126
- Sánchez-Blázquez, P., Peletier, R.F., Jiménez-Vicente, J., Cardiel, N., Cenarro, A.J., Falcón-Barroso, J., Gorgas, J., Selam, S., Vazdekis, A. 2006, *MNRAS*, 371, 703
- Santos, N.C., Israelian, G., & Mayor, M. 2004, *A&A*, 415, 1153
- Schlegel, D.J., Finkbeiner, D.P., & Davis, M. 1998, *ApJ*, 500, 525
- Sekiguchi, M., & Fukugita, M. 2000, *AJ*, 120, 1072
- Skrutskie, M.F., et al. 2006, *AJ*, 131, 1163
- Smalley, B. 2005, *Memorie della Societa Astronomica Italiana Supplementi*, 8, 130
- Smolinski, J.P., et al. 2011, *AJ*, 141, 89
- Sokolov, N. A. 1995, *A&AS*, 110, 553
- Soubiran, C., Le Campion, J.-F., Cayrel de Strobel, G., & Caillo, A. 2010, *A&A*, 515, A111
- Stecher, T.P. 1965, *ApJ*, 142, 1683
- Steinmetz, M., et al. 2006, *AJ*, 132, 1645

- Takeda, Y., Sato, B., Kambe, E., Sadakane, K., & Ohkubo, M. 2002, PASJ, 54, 1041
- Valenti, J.A., & Fischer, D.A. 2005, ApJS, 159, 141
- van Belle, G. T. 2012, A&ARv, 20, 51
- van Belle, G.T., & von Braun, K. 2009, ApJ, 694, 1085
- VandenBerg, D.A., & Clem, J.L. 2003, AJ, 126, 778
- van Leeuwen, F. 2007, A&A, 474, 653
- Weiss, A., & Salaris, M. 1999, A&A, 346, 897
- White, T.R., et al. 2013, MNRAS, 433, 1262
- Wittkowski, M., Aufdenberg, J.P., & Kervella, P. 2004, A&A, 413, 711
- Wittkowski, M., Aufdenberg, J.P., Driebe, T., Roccatagliata, V., Szeifert, T., Wolff, B. 2006, A&A, 460, 855
- Wright, E.L., et al. 2010, AJ, 140, 1868
- Wu, Y., Luo, A., Du, B., Zhao, Y., & Yuan, H. 2014, arXiv:1407.1980
- Xiang, M.-S., et al. 2015, MNRAS, 448, 822
- Yanny, B., et al. 2009, AJ, 137, 4377
- Yi, S., Demarque, P., Kim, Y.-C., Lee, Y.-K., Ree, C.-H., Lejeune, T., Barnes, S. 2001, ApJS, 136, 417
- York, D.G., et al. 2000, AJ, 120, 1579
- Yuan, H.-B., Liu, X.-W., & Xiang, M.-S. 2013, MNRAS, 430, 2188
- Yuan, H.-B., et al. 2015, MNRAS, 448, 855
- Zhang, H.-H., Liu, X.-W., Yuan, H.-B., Zhao, H.-B., Yao, J.-S., Zhang, H.-W., Xiang, M.-S. 2013, RAA, 13, 490
- Zhang, H.-H., Liu, X.-W., Yuan, H.-B., Zhao, H.-B., Yao, J.-S., Zhang, H.-W., Xiang, M.-S., Huang, Y. 2014, RAA, 14, 456

APPENDIX A:

Table A1 presents stars in our sample with multiple angular measurements. It lists angular diameters from different references and the instruments used. The ratios of differences to combined measurement uncertainties, as well as ratios of measurements are also provided.

Table A1. Sample stars with multiple angular diameter measurements

Star	$\theta_{LD} \pm \sigma$ (mas)	Reference	Instrument	$(\theta_{LD,i} - \theta_{LD,1})/\sigma_C^a$	$\theta_{LD,i}/\theta_{LD,1}$
Dwarf stars					
HIP087937	0.952 ± 0.005	B12b	CHARA	0.0	1.00 ± 0.00
	1.004 ± 0.040	Lane et al. (2001)	PTI	1.3	1.05 ± 0.04
HD126660	1.109 ± 0.007	B12a	CHARA	0.0	1.00 ± 0.00
	1.130 ± 0.055	van Belle & von Braun (2009)	PTI	0.4	1.02 ± 0.05
HD142860	1.217 ± 0.005	B12a	CHARA	0.0	1.00 ± 0.00
	1.161 ± 0.054	van Belle & von Braun (2009)	PTI	-1.0	0.95 ± 0.04
HD088230	1.225 ± 0.008	B12b	CHARA	0.0	1.00 ± 0.00
	1.238 ± 0.053	van Belle & von Braun (2009)	PTI	0.2	1.01 ± 0.04
HD109358	1.238 ± 0.030	B12a	CHARA	0.0	1.00 ± 0.00
	1.138 ± 0.055	van Belle & von Braun (2009)	PTI	-1.6	0.92 ± 0.05
HD019373	1.246 ± 0.008	B12a	CHARA	0.0	1.00 ± 0.00
	1.331 ± 0.050	van Belle & von Braun (2009)	PTI	1.7	1.07 ± 0.04
HD097603	1.328 ± 0.009	B12a	CHARA	0.0	1.00 ± 0.00
	1.198 ± 0.053	van Belle & von Braun (2009)	PTI	-2.4	0.90 ± 0.04
HD095735	1.432 ± 0.013	B12b	CHARA	0.0	1.00 ± 0.00
	1.436 ± 0.030	Lane et al. (2001)	PTI	0.1	1.00 ± 0.02
	1.439 ± 0.048	van Belle & von Braun (2009)	PTI	0.1	1.00 ± 0.03
HD030652	1.526 ± 0.004	B12a	CHARA	0.0	1.00 ± 0.00
	1.409 ± 0.048	van Belle & von Braun (2009)	PTI	-2.4	0.92 ± 0.03
HD201092	1.581 ± 0.022	Kervella et al. (2008)	CHARA	0.0	1.00 ± 0.00
	1.666 ± 0.046	van Belle & von Braun (2009)	PTI	1.7	1.05 ± 0.03
HD201091	1.775 ± 0.013	Kervella et al. (2008)	CHARA	0.0	1.00 ± 0.00
	1.628 ± 0.046	van Belle & von Braun (2009)	PTI	-3.1	0.92 ± 0.03
HD026965	1.504 ± 0.006	B12b	CHARA	0.0	1.00 ± 0.00
	1.437 ± 0.039	Demory et al. (2009)	VLT	-1.7	0.96 ± 0.03
HD217014	0.685 ± 0.011	B13	CHARA	0.0	1.00 ± 0.00
	0.748 ± 0.027	Baines et al. (2008)	CHARA	2.2	1.09 ± 0.04
HD103095	0.696 ± 0.005	B12a	CHARA	0.0	1.00 ± 0.00
	0.679 ± 0.015	Creevey et al. (2012)	CHARA	-1.1	0.98 ± 0.02
HD001326	1.005 ± 0.005	B12b	CHARA	0.0	1.00 ± 0.00
	0.988 ± 0.016	Berger et al. (2006)	CHARA	-1.0	0.98 ± 0.02
HD009826	1.114 ± 0.009	Baines et al. (2008)	CHARA	0.0	1.00 ± 0.00
	1.180 ± 0.010	Ligi et al. (2012)	CHARA	4.9	1.06 ± 0.01
HD217987	1.304 ± 0.032	Demory et al. (2009)	VLT	0.0	1.00 ± 0.00
	1.388 ± 0.040	Ségransan et al. (2003)	VLT	1.6	1.06 ± 0.04
HD128621	6.000 ± 0.021 ^b	Bigot et al. (2006)	VLT	0.0	1.00 ± 0.00
	6.001 ± 0.034	Kervella et al. (2003)	VLT	0.0	1.00 ± 0.01
HD121370	2.269 ± 0.025	M03	Mark III	0.0	1.00 ± 0.00
	2.170 ± 0.030	Nordgren et al. (2001)	Mark III	-2.5	0.96 ± 0.02
	2.280 ± 0.070	Nordgren et al. (2001)	NPOI	0.1	1.00 ± 0.03
	2.200 ± 0.027	Thévenin et al. (2005)	VLT	-1.9	0.97 ± 0.02
HD150680	2.367 ± 0.051	M03	Mark III	0.0	1.00 ± 0.00
	2.330 ± 0.050	Nordgren et al. (2001)	Mark III	-0.5	0.98 ± 0.03
	2.490 ± 0.090	Nordgren et al. (2001)	NPOI	1.2	1.05 ± 0.04
HD061421	5.446 ± 0.054	M03	Mark III	0.0	1.00 ± 0.00
	5.460 ± 0.080	Nordgren et al. (2001)	Mark III	0.1	1.00 ± 0.02
	5.430 ± 0.070	Nordgren et al. (2001)	NPOI	-0.2	1.00 ± 0.02
	5.390 ± 0.030 ^b	Chiavassa et al. (2012)	VLT	-0.9	0.99 ± 0.01
Giant stars					
HD133208	2.477 ± 0.065	M03	Mark III	0.0	1.00 ± 0.00
	2.520 ± 0.040	Baines et al. (2010)	PTI	0.6	1.02 ± 0.03
	2.480 ± 0.080	Baines et al. (2010)	NPOI	0.0	1.00 ± 0.04
HD216131	2.496 ± 0.040	M03	Mark III	0.0	1.00 ± 0.00
	2.460 ± 0.060	Baines et al. (2010)	PTI	-0.5	0.96 ± 0.03
	2.500 ± 0.080	Baines et al. (2010)	NPOI	0.0	1.00 ± 0.04
HD096833	4.120 ± 0.041	M03	Mark III	0.0	1.00 ± 0.00
	4.110 ± 0.040	Baines et al. (2010)	PTI	-0.2	1.00 ± 0.01
	4.080 ± 0.070	Baines et al. (2010)	NPOI	-0.5	0.99 ± 0.02
HD189319	6.225 ± 0.062	M03	Mark III	0.0	1.00 ± 0.00
	6.197 ± 0.035	Wittkowski et al. (2006)	NPOI	-0.4	1.00 ± 0.01
	6.170 ± 0.012	Wittkowski et al. (2006)	VLT	-0.9	0.99 ± 0.01

^a We define the combined errors as $\sigma_C = (\sigma_{LD,1}^2 + \sigma_{LD,i}^2)^{1/2}$ ^b Values of θ_{LD} are derived with 3D model atmospheres. Others are all derived with 1D model atmospheres.